Applied Thermal Engineering 248 (2024) 123335

Contents lists available at ScienceDirect

Applied Thermal Engineering

journal homepage: www.elsevier.com/locate/ate

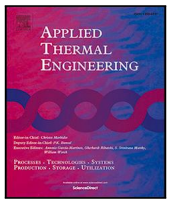

Research Paper

Experimental study of an on-grid hybrid solar air conditioner with evaporative pre-cooling of condenser inlet air

P. Martínez *, M. Lucas, F.J. Aguilar, J. Ruiz, P.V. Quiles

Instituto de Investigación en Ingeniería de Elche, Universidad Miguel Hernández de Elche, Avda. de la Universidad, s/n, 03202 Elche, Spain

ARTICLE INFO

Keywords:
Solar refrigeration
Evaporative cooling
Efficiency
Photovoltaics

ABSTRACT

This paper presents an experimental study of a split type solar air conditioning system with evaporative pre-cooling at the condenser. The main objective of this research is to evaluate the thermal and electrical performance of the system under hot summer conditions in a Mediterranean climate. Previous studies have separately shown the benefits of both condenser inlet air pre-cooling and photovoltaic solar cooling. The novelty of this work will be the study of the coupling of these two techniques in a real installation, where the viability of the system depends on the component-level design and the operating conditions, since weather variables such as ambient temperature, relative humidity and solar radiation significantly affect the thermal behaviour of the refrigeration cycle, the evaporative pre-cooling capacity and the performance of the photovoltaic panels. Experimental tests were carried out over a summer season to evaluate the behaviour of the system and to obtain performance correlations validated with experimental data. These correlations will allow the modelling of the system and will be used to carry out an economic and environmental feasibility study of the proposed hybrid solar air conditioning system. The results show that a 100 mm-thick evaporative pad achieved an average evaporative cooling efficiency for all tests performed of $\varepsilon_{evap} = 67.4\,\%$, reducing the air inlet temperature to the condenser by around 6 °C. This resulted in an 18.3 % improvement in the *EER* of the air conditioner. In addition, the use of evaporative pre-cooling resulted in a significant 23 % reduction in peak power consumption. The study also evaluated the impact of the air pressure drop caused by the evaporative pad when not in use, with results favouring its installation. The system achieved a solar contribution of more than 30 % under different solar radiation conditions when using pre-cooling, compared to 25 % with a standard condenser. In addition, the combination of photovoltaic contribution and evaporative pre-cooling reduced energy consumption by 43 %.

1. Introduction

Air conditioning accounts for 20 % of global electricity consumption in buildings and 10 % of global electricity consumption. The increasing use of air conditioning in residential and commercial buildings will be one of the main drivers of global electricity demand growth over the next few decades, [1]. Optimising the energy performance of a building starts with the design and construction of a near-zero energy passive building from an architectural point of view. The next steps are the use of energy saving devices to reduce the amount of energy required for operation and the incorporation of renewable energy technologies in various applications, [2]. Prioritising energy efficiency reflects the fact that the most cost-effective and environmentally friendly form of energy is the one that does not require production, [3]. Continuing this line of argument, this paper deals with a proposal to improve the energy efficiency of an air conditioning system and the integration of photovoltaic energy in its operation.

The use of solar energy for air conditioning is based on a fundamental principle: matching the availability of solar radiation with the cooling demand. The main objective is to develop cost-effective solar air conditioning systems. Although a number of technical solutions have been studied for the combination of solar energy and air conditioning, this technology is still at an early stage of development. According to the International Energy Agency's Task 53 on new generation solar cooling and heating systems, Mugnier et al. [4] stated that photovoltaic (PV) driven compression chillers are currently the most promising solar solutions, especially for small to medium sized units (<50 kW cooling), and are close to market readiness. Previously, it appeared that solar cooling systems had the greatest potential for deployment in large buildings with central air conditioning systems,

* Corresponding author.
E-mail address: pedro.martinez@umh.es (P. Martínez).
URL: https://www.umh.es (P. Martínez).

https://doi.org/10.1016/j.applthermaleng.2024.123335
Received 7 November 2023; Received in revised form 5 April 2024; Accepted 1 May 2024
Available online 5 May 2024

Nomenclature

AC	air conditioning
A_{total}	total area of the solar panels (m^2)
COP	coefficient of performance (-)
EER	energy efficiency ratio (-)
E_{grid}	daily energy consumption of the AC unit from the grid ($kWh\,d^{-1}$)
E_{pv}	daily energy consumption of the AC unit from the photovoltaic panels ($kWh\,d^{-1}$)
E_{total}	total energy consumption of the AC unit over a day ($kWh\,d^{-1}$)
E_{unit}	daily thermal energy supplied by the AC unit ($kWh\,d^{-1}$)
G	solar irradiance ($W\,m^{-2}$)
h	enthalpy ($kJ\,kg^{-1}$)
I	electric current (A)
k	confidence level coverage factor (-)
LF	load factor of AC unit (%)
$\dot{m}$	mass flow rate ($kg\,s^{-1}$)
n	number of data points per day per sensor (-)
$\dot{Q}$	useful thermal capacity (heating/cooling) (W)
r	correlation coefficient (-)
RH	relative humidity (%)
SC	solar contribution (%)
SPF	seasonal performance factor (-)
T	temperature (°C)
T_{wb}	air wet bulb temperature (°C)
ΔT_a	air temperature drop (°C)
$\Delta T_{a,max}$	maximum air temperature drop (°C)
Δt	time interval for data acquisition (s)
u	standard, combined or expanded uncertainty
v	velocity ($m\,s^{-1}$)
V	electric voltage (V)
$\dot{V}$	volume flow rate ($m^3\,kg^{-1}$)
$\dot{W}$	electrical power (W)
W_d	wind direction (°)
W_v	wind velocity ($m\,s^{-1}$)

Greek symbols

ε_{evap}	evaporative cooling efficiency (%)
η	electrical efficiency (%)
ω	humidity ratio of moist air ($kg_w\,kg_a{}^{-1}$)
$\cos\phi$	electrical power factor (-)
ρ	density ($kg\,m^{-3}$)

Subscripts

1, 6	refrigerant at evaporator outlet/inlet
2, 3	refrigerant at compressor inlet/outlet
4, 5	refrigerant at condenser inlet/outlet
a	air
ac	alternating current
acc	transducer or probe accuracy
amb	ambient air
avg	average value
bleed	bleed-off water
comp	reciprocating compressor of the AC unit
da	data acquisition unit
dc	direct current
evap	evaporated by the pre-cooling pads
grid	electricity grid
in	evaporative pad inlet air flow
meas	measurement
mid	air flow between evaporative pad and condenser
out	condenser outlet air flow
pv	photovoltaic panels
rd	data readout
ref	R410A refrigerant
supply	total fresh water consumption
syst	whole system (AC unit + photovoltaic)
total	total consumption of the AC unit
tr	transducer or probe
unit	air conditioning unit
w	water

mainly due to the progress of solar thermal cooling solutions in this particular sector. However, the landscape has changed because of the considerable increase in demand for cooling in the small residential and small commercial sectors, combined with a considerable reduction in the cost of PV panels. As a result, the market dynamics have changed.

A number of recent experimental studies and simulations have highlighted the significant potential of photovoltaic (PV) cooling. Among the large number of works available in the literature on this topic, a few have been selected on the basis of their coincidence with the power range developed in the present research. Aguilar et al. [5] tested a heat pump with a cooling capacity of 3.52 kW, which was simultaneously powered by three 235 Wp photovoltaic panels and the electrical grid during the Spanish hot season. The cooling system was installed in an office, and both the solar contribution and the production factor reached about 65 %. Opoku et al. [6] investigated the performance of a hybrid solar PV system with batteries and grid-powered air conditioner, consisting of a 1040 Wp solar PV array with a 200 Ah, 24 V battery configuration, for daytime cooling of an office in a hot and humid climate over the course of a year. The monthly average solar fraction was found to be 51 % ± 9 % for an air conditioner with a nominal cooling capacity of 2.5 kW and a maximum power consumption of about 1.19 kW. Lorenzo et al. [7] investigated the benefits of incorporating two control algorithms specifically designed for the compressor of a 3.4 kW stand-alone PV heat pump prototype operating in cooling mode without the use of batteries. The results showed a performance ratio between 0.17 and 0.5, an energy efficiency ratio (*EER*) between 2.51 and 3.06 and a seasonal performance factor (*SPF*) between 2.51 and 3.01. Chen et al. [8] investigate on the effectiveness of photovoltaic air conditioning systems in office buildings. The study found that the PV AC system can quickly regulate the room temperature within a set range of ±0.9 °C, and provide 114 %, 73 % and 188 % of the energy required by the AC system in the cooling, heating, and annual operating periods, respectively. Saâd et al. [9] carried out an experimental study of a hybrid air conditioner powered by a photovoltaic system and the grid to analyse its energy performance. The test setup consisted of an air conditioner with a nominal cooling capacity of 2.63 kW and a PV system with four 335 Wp panels connected through a 1.3 kW inverter. The results showed that the solar contribution factor was 50 % in winter and 73 % in summer. Ayadi et al. [10] presented an experimental setup that uses solar energy to power an air conditioner. The system was tested in two scenarios: on-grid and off-grid. The results showed that the solar fraction was higher during periods of higher demand and ambient temperature, and the system maintained operation solely on

PV power during the studied clear sky day load profile. The economic analysis showed an attractive simple local payback period of 6.91 and 6.4 years for on-grid and off-grid systems respectively. Finally, Li et al. [11] conducted a study on the potential of photovoltaic air conditioning systems for summer cooling in mainland China. The study provided valuable insights into the potential of PV AC systems as a sustainable and cost-effective cooling solution and proposed a generalised design guide for PV AC systems.

The use of pre-cooling of the incoming air to the condenser of an air conditioning system has proven to be a consistent strategy to improve its efficiency. Several authors have discussed its practical implementation and quantified the associated energy improvement. He et al. [12] reviewed the types of evaporative pre-cooling, related mathematical models, studies evaluating their performance and empirical relationships. Ibrahim et al. [13] considered the use of condensate to pre-cool the condenser air in a split-type air conditioning system with a cooling capacity of 1.5 ton, in order to sensibly reduce the temperature of air entering the condenser. A 4 °C decrease in the temperature of the air entering the condenser was found, resulting in a 21.4 % increase in *COP* with an enhanced cooling capacity. Yu et al. [14] analysed the cooling effectiveness of mist in pre-cooling air entering the condenser of an air-cooled chiller. The chiller had a cooling capacity of 282 kW and operated with a mist system in two different modes: the first was the normal mode with head pressure control, and the second was the VSD mode with variable speed control of the condenser fans. In a subtropical climate, mist pre-cooling of the condenser air increased the *COP* of the chiller from 0.36–8.86 % and from 0.34–10.19 % in the normal and VSD modes, respectively. Yang et al. [15] investigated the effectiveness of a spray evaporative cooling system in improving the performance of an air-cooled chiller in refrigeration applications. The experimental results showed a reduction in compressor power consumption and a 4 % to 8 % increase in the *COP* of the air-cooled chiller following application of the spray evaporative cooling system. Furthermore, the spray cooling system significantly reduced the power consumption of air-cooled chillers, with energy savings ranging from 2.4 % to 13.5 %. More recently, Jacob et al. [16] have discussed the need for alternative cooling systems to meet future demand and reduce environmental impact, particularly in residential air conditioning. A hybrid evaporative-vapour compression cycle, which combines adiabatic latent cooling with the vapour compression cycle, was presented as one such alternative. The results showed that the proposed system is most effective in hot, dry climates, with energy savings in excess of 20 %. Gupta et al. [17] proposed an innovative approach to address the environmental impact of refrigeration and air conditioning systems by integrating evaporative cooling and passive cooling in a 1.5 ton split air conditioner. The results showed significant thermodynamic performance improvements, with a maximum coefficient of performance improvement of 68.7 % observed at 44 °C and 20 % relative humidity. Atmaca et al. [18] investigated the performance of a split air conditioner with an evaporatively cooled condenser compared to a conventional air-cooled condenser. Tests under different environmental conditions showed that evaporative cooling significantly improved energy efficiency. Specifically, with evaporative cooling, the coefficient of performance increased by 10.2–35.3 %, the cooling capacity increased by 5.8–18.6 % and the total power consumption decreased by 4.0–12.4 %. Gupta et al. [19] conducted a thorough thermo-economic evaluation of a 5.25 kW capacity split air conditioner integrated with direct evaporative cooling to assess its performance, energy consumption, coefficient of performance and economic viability. The Box Behnken design technique was used for multi-objective optimisation, resulting in a significant increase in *COP* up to 68.9 % and a reduction in total cost rate and total exergy destruction by 26.1 % and 57.2 % respectively.

As a direct precursor to the current work, Martínez et al. [20] investigated the improvement of energy efficiency by using evaporative cooling pads of different thicknesses for pre-cooling at the condenser unit of an air conditioning system with a cooling capacity of 2.5 kW. The experimental results showed that the addition of an evaporative cooling pad with a thickness of approximately 100 mm resulted in the highest overall *COP*. This reduced compressor power consumption by 11.4 %, increased cooling capacity by 1.8 % and improved overall *COP* by 10.6 %. Similarly, Harby and Al-Amri [21] used cellulose pads of different thicknesses as a condenser pre-cooling system to study the performance improvement and energy savings of a 5.2 kW conventional split air conditioner. They also found that the optimal thickness of the pad was 100 mm.

The experimental results show that using this particular thickness resulted in a significant reduction in energy consumption, ranging from 15 to 22 %, while improving the overall *COP* by 29 to 53 %. A review of the literature revealed that numerous studies have focused on investigating the effect of air pre-cooling on the thermal behaviour of refrigeration cycles. However, no references have been found where air pre-cooling is combined with the use of solar energy.

As seen above, a literature search reveals many references to air conditioning systems using evaporative condenser cooling and references to photovoltaic cooling systems. Previous research suggests that both condenser inlet air pre-cooling and photovoltaic cooling are very promising, as they have achieved very good results independently. However, very few references have been found that investigate the coupling of these two techniques in a real installation and provide experimental data on the performance of a hybrid solar air conditioning system with condenser inlet air pre-cooling. One of the few recent research studies dealing with such hybrid systems, but using a different evaporative cooling technique, is Yang et al. [22], which describes a proposed ultra-efficient air conditioner with smart evaporative cooling ventilation and photovoltaics for residential use in (sub)tropical areas.

The objective of this work is the experimental investigation of the thermal and electrical performance of a hybrid solar system with evaporative pre-cooling of the condenser inlet air under hot summer conditions in a Mediterranean climate. There are a number of issues related to their coupling in a real installation that make their study interesting, and both the operating conditions of the installation and its design at component level are key to assessing its viability. For example, weather variables (ambient temperature, relative humidity and solar radiation) affect the thermal behaviour of the refrigeration cycle, the evaporative pre-cooling capacity and the performance of the photovoltaic panels. Therefore, the study of this particular hybrid solar air conditioner in a real installation, with the aim of obtaining performance correlations validated with experimental data, will be the main novelty of this work. These correlations will allow the modelling of the system and will be used to carry out an economic and environmental feasibility study of the proposed hybrid solar air conditioner.

This paper is structured as follows. Section 2 provides a brief description of the ad hoc experimental test facility and the experimental procedure. The definition of the design parameters and the key performance indicators of the solar air conditioner and the uncertainty analysis are presented in Section 3. Section 4 is dedicated to the description of the experimental results, evaluating the benefits in terms of peak power and daily energy obtained. First, a comparison is made between the different operating modes for similar environmental conditions. Then, the results of all the daily tests carried out during a whole summer season and including different environmental operating conditions are presented. Section 5 summarises the most relevant results obtained in this research work.

2. Experimental methodology

2.1. Experimental setup

For the experimental tests, a compact prototype of a solar cooling system with evaporative pre-cooling pads was designed and built using commercially available components (see Fig. 1). The prototype consisted mainly of three sub-systems: a residential split air conditioner

Fig. 1. Prototype of a solar cooling system with evaporative pre-cooling pads.

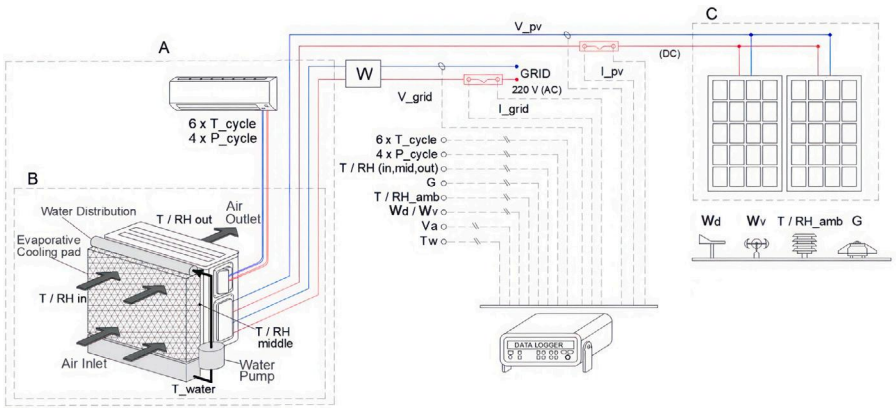

Fig. 2. Schematic diagram of the experimental prototype with subsystems and instrumentation.

(sub-system A), an adiabatic pre-cooling system of the inlet air to the condenser using commercially available corrugated cellulose evaporative pads (sub-system B), and two photovoltaic modules for power supply (sub-system C), as shown in Fig. 2.

The Kaysun air conditioning unit consists of a condenser unit (model KAE-PV 35 DN5) and an evaporator unit (model KAY-PV 35 DN5). The condenser was used as the outdoor unit in the experimental test. The air conditioner has a rated cooling capacity of 3660 W and uses R410 A refrigerant. It is driven by a 980 W DC rotary inverter compressor (model DA130M1C-31FZ), which has been fully thermally insulated to ensure quasi-adiabatic compression. The copper pipes carrying the refrigerant are also thermally insulated, as is the capillary expansion tube, where the insulation has been improved to guarantee an isoenthalpic expansion process.

A solar installation consisting of two PEIMAR SG360M photovoltaic modules, with the technical specifications given in Table 1, is used to supply a significant part of the electrical energy consumed by the air conditioning system. The panels have been installed on the flat roof of the laboratory, as shown in Fig. 1, with a south orientation (0° azimuth) and an inclination angle of 30° to the horizontal, in order to optimise their performance in summer.

The air conditioner is electrically powered by simultaneous connection to the mains (230 Vac) and directly to the photovoltaic panels (24 Vdc) without the need for an external inverter. The two power sources operate in parallel and are added together to provide all the electrical energy required by the air conditioner. In this way, the AC unit always has enough power for stable operation, regardless of variations in solar radiation. Internally, this AC unit has an inverter that converts the energy from the 230 Vac mains to 200–300 Vdc to drive the compressor at different speeds. The integration of the photovoltaic

Table 1
Technical specifications of PEIMAR SG360M photovoltaic modules.

Maximum power	P_{mpp} (W)	360 W
Tolerance	P_{mpp}	0/+5 W
Dimensions	mm	1957×992×40
Number of cells	N	72
Cell type (mono PERC)	mm	156×156
Module efficiency	%	18.54
Short circuit current	I_{sc} (A)	10.09
Open circuit voltage	V_{oc} (V)	46.6
Nominal current	I_{mpp} (A)	9.48
Nominal voltage	U_{mpp} (V)	38
Temp. coeff. of I_{sc}, α	I_{sc} (%/°C)	0.047
Temp. coeff. of V_{oc}, β	V_{oc} (%/°C)	−0.32
Temp. coeff. of P_{max}, γ	P_{max} (%/°C)	−0.40

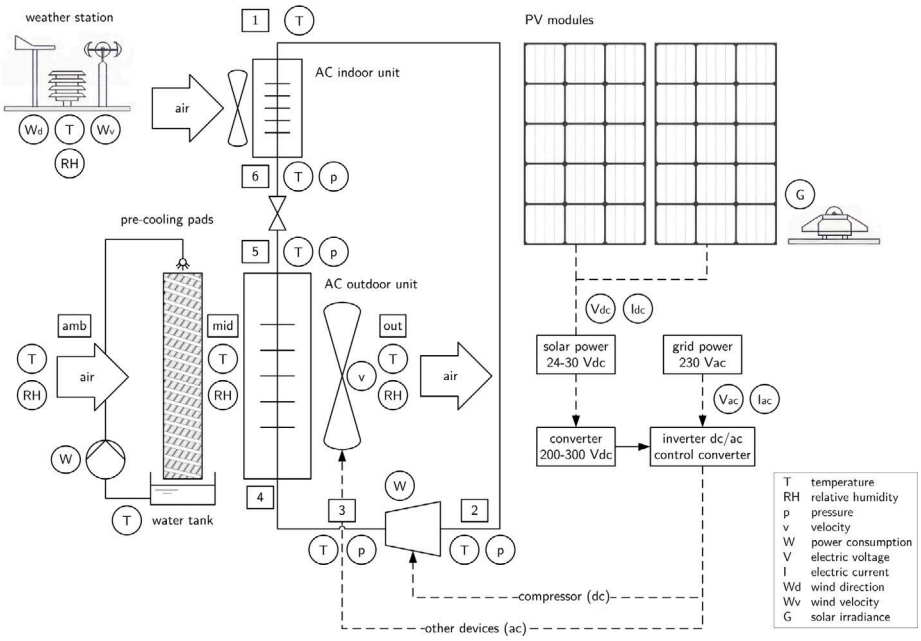

Fig. 3. Schematic diagram of the test facility showing interconnection of equipment and location of instrumentation.

energy takes place before the connection to the compressor, through a power converter that raises the 24 Vdc of the panels to 200–300 Vdc. During the hours of maximum solar radiation, the production of PV energy is sufficient to supply the entire system. At this time, the PV energy is the main source of power due to the impedance difference between the two sources (PV and grid). Only when the PV power is insufficient is the grid power used.

Fig. 1 shows the pre-cooling system, which consists of a stainless steel frame that can hold one to three Munters corrugated cellulose evaporative cooling pads, in particular pad model CELdek® 5090-15. The evaporative pads are kept wet by a hydraulic circuit driven by a small recirculating water pump that provides a constant flow of water to the top of the frame along the entire length of the pads. Holes drilled in the top of the frame allow Munters recommended water flow to be evenly distributed by gravity over the fill of the evaporative pads. On the other hand, the air flow that passes through the pads and comes into contact with the wet fill undergoes an evaporative cooling process, taking some of the feed water with it. The remaining non-evaporated water is collected by gravity in a tank at the bottom of the pads, where the suction of the recirculation pump is located, which collects the water and returns it to the pads. Figs. 2 and 3 show a schematic diagram of the complete installation with all the components of the laboratory prototype, showing both the water and air flows involved in the investigation and the location of the instrumentation used in the experimental tests.

A number of additional controls were installed on the laboratory prototype to ensure continuous control and monitoring of the test development. This was achieved by automating the water replenishment of the system with an additional tank, which was used to continuously maintain the water level and also to determine how much water was being used. In addition, two mobile phones were installed to monitor the water levels in the tanks via their cameras and to report the general status of the system for safety reasons. An Arduino UNO microcontroller board equipped with an infrared emitter was installed to control the on/off and temperature set points of the air conditioning system so that it could be controlled remotely. Generic desktop remote control software was used to control the PC that collected the information from the data acquisition system. With all these improvements it was possible to run a significant number of tests remotely.

2.2. Hydraulic design

In order to perform the hydraulic design of the pre-cooling system, it was first necessary to define the number of pads to be used in the tests. On the basis of a previous experimental energy efficiency study carried out on an air conditioning unit with similar characteristics to the one used in this study and using the same type of evaporative pads [20], the results showed that the optimum total thickness of the evaporative section was 100 mm in order to obtain an adequate amount of pre-cooling of the air flow, without causing an excessive loss of pressure in the air flow and a consequent reduction in its flow rate, which would penalise the condenser's ability to dissipate heat to the environment. For this reason, it was decided to mount two 50 mm-thick pads in series.

The recirculation pump was sized by estimating the water flow required to keep the cellulosic media in the pad fully wetted. According to the manufacturer's recommendations, a minimum water flow is required to achieve sufficient wetting and optimal performance. To calculate the distribution flow rate, a specific water flow rate of 90 $L\,min^{-1}$ per m^2 top surface was considered for pad type CELdek® 5090-15.

Taking into account the actual dimensions of the two 50 mm-thick installed pads of 100×800×585 mm (depth × length × height), the distribution flow rate to the total top surface of the pads was calculated to be 429.8 $L\,h^{-1}$.

To maintain the optimal mineral concentration in the water, a bleed-off water flow rate must be constantly drained off by the pump. This rate should be added to the previously calculated distribution flow rate. The bleed-off rate was calculated as 1.9 $L\,h^{-1}$ based on the analysis of the fresh water supplied to the pre-cooling system and using a water quality chart provided by the manufacturer, therefore the pump capacity was calculated as 431.7 $L\,h^{-1}$.

To select a suitable pump, the hydraulic losses in the recirculation circuit were calculated, taking into account the previously calculated water flow rate, the height of the pads, the diameter and length of the distribution pipes and the additional losses caused by fittings. It was found that the pump required less than 10 W to do its job, assuming a pump efficiency of 20 %.

A calculation based on the most demanding environmental conditions in which the pre-cooling system is likely to operate, considering a temperature of $T_{amb} = 30\,°C$ and a relative humidity of $RH_{amb} = 30\,\%$,

has been made to calculate the water evaporation rate and the total water supply requirement. Thus, the water evaporation rate can be obtained as follows:

$$T_{wb,amb} = T_{wb}\left(T_{amb}, RH_{amb}\right) \quad (1)$$

$$T_{mid} = T_{amb} - \varepsilon_{evap}\left(T_{amb} - T_{wb,amb}\right) \quad (2)$$

$$\dot{V}_{w,evap} = \frac{\rho_a \dot{V}_a}{\rho_w}\left(\omega\left(T_{mid}, T_{wb,amb}\right) - \omega\left(T_{amb}, RH_{amb}\right)\right) = 9.6\,\mathrm{L\,h^{-1}} \quad (3)$$

where a value of $\varepsilon_{evap} = 88.5\,\%$ has been estimated from the evaporative cooling efficiency diagram for pad type CELdek® 5090-15 provided by the manufacturer. Then, in Section 4 the evaporative cooling efficiency will be recalculated experimentally to determine the actual value obtained for our specific pre-cooling system installation.

The total estimated fresh water consumption of the prototype can therefore be calculated by summing $\dot{V}_{w,evap}$ and the bleed-off flow rate, giving:

$$\dot{V}_{w,supply} = \dot{V}_{w,evap} + \dot{V}_{w,bleed} = 11.5\,\mathrm{L\,h^{-1}} \quad (4)$$

2.3. Sensoring

A variety of sensors and measurement equipment were used to study the thermal and electrical behaviour of the system. Firstly, the environmental conditions were recorded using ambient air temperature and relative humidity sensors and wind speed and direction sensors, all located in a weather station on the roof of the laboratory where the tests were carried out, next to the solar installation. Solar radiation was measured for the entire solar spectrum using an ISO-first-class pyranometer, installed at the same level as the photovoltaic modules.

Four pressure transducers were used to measure the characteristic states of the refrigeration cycle. It is usual to use only two pressure transducers for this characterisation, but it was preferred to double these sensors to determine the pressure loss in the heat exchangers (condenser and evaporator). In addition, six RTD-Pt100 temperature sensors were installed on the copper pipes. Temperature and humidity sensors were placed at the front and back of the cooling pads and at the condenser air outlet to monitor the air temperature and relative humidity through the system to analyse the psychrometric changes of the air in the pre-cooling section and as it passes through the condenser.

For the electrical parameters, DC voltages were measured directly and the DC current of both PV panels was determined from the voltage drop value generated across a dedicated calibrated shunt resistor. True RMS transducers were used to measure the AC voltages and currents.

A Keysight Technologies DAQ970A data acquisition system, equipped with two DAQM901A channel multiplexer modules (2/4 wire) supporting up to 44 inputs, with built-in 6 $\frac{1}{2}$ digit DMM, 50.000 readings per second and programmable gain for each individual channel, was used to record all the measurements taken during the tests. The frequency of data acquisition was every 10 s. Control of the start and stop of data acquisition and data storage was performed from a PC with BechVue software installed to establish communication with the data acquisition system. The configuration of each channel and the adjustment of its gain and offset depending on the type of probe connected was created and compiled using the BechVue software. Table 2 shows a summary of the technical specifications and accuracy of the different types of probes and measurement equipment installed in the laboratory prototype where the tests were carried out.

2.4. Experimental procedure

Experimental tests were carried out over an entire summer season, covering the full range of environmental conditions for a Mediterranean climate, with ambient temperatures ranging from 20 °C to 35 °C and relative humidities ranging from 30 % to 80 %, in order to evaluate the behaviour of the system and obtain performance correlations validated with experimental data. All tests were carried out with the evaporator fan running at full load to evaluate the performance of the solar air conditioning system with and without pre-cooling. Fig. 4 shows the steps involved in a daily test, starting at 7.30 am with the activation of the water recirculation pump (if necessary) responsible for wetting the evaporative pads. To ensure complete wetting of the evaporative pads, the water supply is maintained for 30 min before the air conditioning unit is switched on at 8.00 am. From this time until 8.00 pm, the AC unit runs continuously at a load factor of $LF = 100\,\%$, where LF is defined as the ratio of actual to maximum cooling capacity of the air conditioning unit. A preliminary analysis of the recorded data showed that it takes about 30 min after the air conditioning unit is switched on for the system to reach stable operating conditions for the temperatures and pressures of the refrigeration cycle, which was taken into account in the hourly averaging of the values recorded by the sensors. Data curation was carried out by filtering the measurements collected by the data logger and by taking hourly and daily averages of all the values recorded during the tests to finally obtain the values of the key performance parameters using the equations in Section 3.

Two principal scenarios were used for the experimental work. The base case was the operation of the split air conditioning system, simultaneously powered by the grid and the photovoltaic panels (operating mode 1: AC + PV). In the second mode, evaporative pads were added and water recirculation was activated to provide pre-cooling of the air flow passing through the condenser (operating mode 2: AC + wet pads & pre-cooling + PV).

One of the disadvantages of using pre-cooling systems based on evaporative pads is the additional pressure drop that they can cause in the condenser air flow, even when the water recirculation is deactivated, because it is not interesting to perform the air pre-cooling, for example in the winter season when the pump heat is operating in heating mode. In order to evaluate the possible negative effect of the presence of the dry pads on the air inlet to the condenser, it was considered appropriate to include a third operating mode for the air conditioning system, in which the evaporative pads are still installed but the water circulation is deactivated so that no pre-cooling is achieved (operating mode 3: AC + dry pads & no pre-cooling + PV). Comparative results of leaving the pads installed or removing them from the system in situations where they are not required are shown in Section 4.3.

3. Evaluation index

3.1. Key performance indicators of the solar air conditioner

In order to characterise the performance of the system, the following key performance indicators are defined. They can be calculated either on a power basis or on an energy basis.

The consumption of solar energy by the air conditioning system has been calculated as follows:

$$\dot{W}_{pv} = I_{pv} V_{pv} \quad (5)$$

The electrical efficiency of PV modules, which is the ratio of electrical power generation to total available solar power, is defined as:

$$\eta_{pv} = \frac{\dot{W}_{pv}}{GA} \quad (6)$$

The power consumption of the AC unit from the grid is:

$$\dot{W}_{grid} = I_{grid} V_{grid} \quad (7)$$

The total power consumption of the air conditioning system, including the consumption of the condenser and evaporator fans, is calculated by adding the above two power indicators as follows:

$$\dot{W}_{total} = \dot{W}_{pv} + \dot{W}_{grid} \quad (8)$$

Table 2
Technical specifications and accuracy of the different types of probes and instruments installed in the experimental test facility.

Measurement	Brand/model	Measuring device	Measuring range	Accuracy
Refrigerant temperature	TC Direct, Pt-100 class 1/3 DIN	RTD 4 W	−50 to +200 °C	±0.15 °C
Refrigerant low pressure	Johnson Controls, P499ACS-404	Pressure transducer	0 to 30 bar	±1 % max
Refrigerant high pressure	Johnson Controls, P499ACS-405	Pressure transducer	0 to 50 bar	±1 % max
Water temperature	Desin Instruments, Pt-100 class 1/10 DIN	RTD 4 W	−20 to +250 °C	±0.05 °C
Air velocity	Osaka, ANE-MS-distan	Hot wire anemometer	0 to 30 m s^{-1}	±0.04 m s^{-1} + 3 % mv
Air temperature	E+E Elektronik, EE210P-HTCB	Capacitive sensor	−40 to +60 °C	±0.2 °C
Air relative humidity	E+E Elektronik, EE210P-HTCB	Capacitive sensor	0 % to 100 %	±2.5 %
Wind direction	Wind Sentry, model 03002L	Balanced vane	360°/352° mech./elec.	±10°/5° for 1.3/1.9 m s^{-1}
Wind speed	Wind Sentry, model 03002L	Cup anemometer	0 to 50 m s^{-1}	±1.1 m s^{-1}
Solar radiation	Kipp & Zonen, model CM-6B	Pyranometer	0–1400 W m^{-2}	<1.2 %
Ambient air temperature	Young, model 41382LC2	RTD 4 W	−50 to +50 °C	±0.3 °C
Ambient air relative humidity	Young, model 41382LC2	Capacitive sensor	0 % to 100 %	±1 %
PV voltage	Keysight, DAQ970A & DAQM901A	Direct	100 mV to 300 V	±0.003 %
PV current	Zurk	Shunt resistor	0–10 A	±0.5 %
AC voltage transducer	Phoenix Contact, MCR-VAC-UI-O-DC	Converter	0–370 Vac	±0.5 %
AC current transducer	Phoenix Contact, MCR-S-1/5-UI-DCI-NC	Converter	0–11 A	±0.5 %

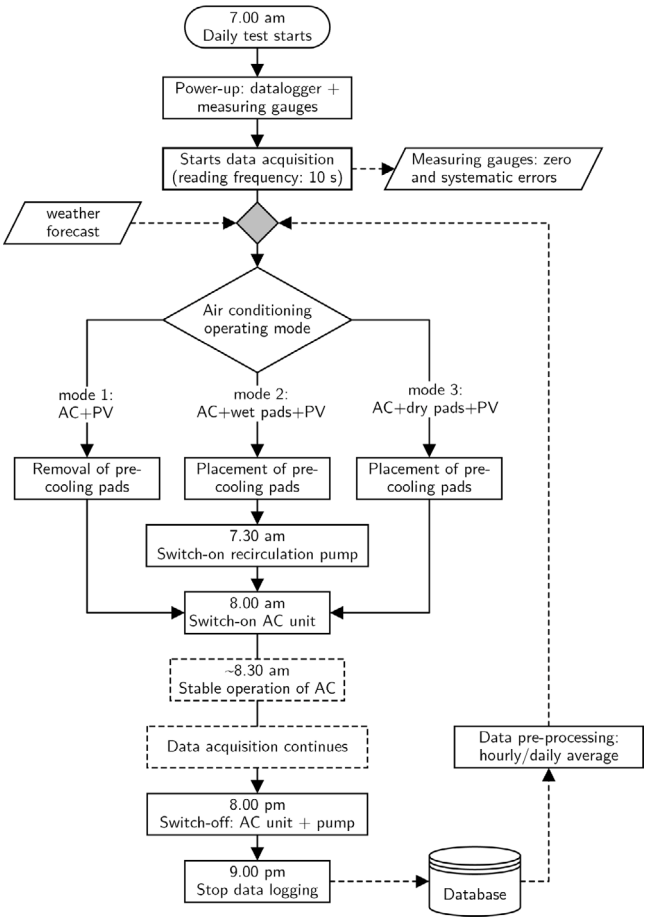

Fig. 4. Flowchart showing the decisions and steps involved in performing a daily test.

To analyse the refrigeration cycle, it is useful to determine the power consumed by the compressor alone using the following formula:

$$\dot{W}_{comp} = I_{comp} V_{grid} \cos\phi \tag{9}$$

For energy analysis, power data in kW can be converted to energy data in kWh by summing the products of the readings obtained for each instantaneous magnitude and the time interval between two successive measurements. In this way, the energy supplied by the grid and the energy supplied by the photovoltaic panels are calculated using the following equations:

$$E_{grid} = \sum_{i}^{n} \dot{W}_{grid,i} \Delta t \tag{10}$$

$$E_{pv} = \sum_{i}^{n} \dot{W}_{pv,i} \Delta t \tag{11}$$

The total energy consumption of the air conditioning system can be calculated by:

$$E_{total} = E_{pv} + E_{grid} \tag{12}$$

The solar contribution, defined as the ratio of the energy produced by the solar panels to the total energy consumed by the equipment, is calculated as:

$$SC(\%) = 100 \frac{E_{pv}}{E_{total}} \tag{13}$$

In order to evaluate the efficiency of the air conditioning system, it is necessary to calculate the useful thermal energy delivered by the equipment. The first step is to determine the refrigerant mass flow, which is obtained by dividing the power consumption of the compressor by the specific work. The specific work is the difference in enthalpy between the inlet and outlet of the compressor, taking into account a compressor loss of 5 %, as recommended by the manufacturer. As a result, an expression similar to that described in Aguilar et al. [23], adjusted with experimental data, was used to calculate the mass flow rate of refrigerant:

$$\dot{m}_{ref} = \frac{0.93 \dot{W}_{comp}}{h_2 - h_1} \tag{14}$$

Once the refrigerant mass flow rate is known, the useful thermal power is calculated by multiplying the mass flow by the enthalpy difference between the evaporator inlet and outlet:

$$\dot{Q} = \dot{m}_{ref}(h_1 - h_6) \tag{15}$$

The points where the refrigerant conditions were measured are shown in Fig. 2. The Engineering Equation Solver software [24], which includes a database of refrigerants and their properties, was used to repeat the above process for each recorded data point. The useful thermal energy delivered during a typical day (E_{unit}) is obtained by summing the product of the useful power at each instant and the time elapsed between data readings, expressed as:

$$E_{unit} = \sum_{i}^{n} \dot{Q}_i \Delta t \tag{16}$$

The energy efficiency of the air conditioner (EER_{unit}) and the energy efficiency of the system (EER_{syst}) are calculated according to the

following expressions, where in the second case only the non-renewable energy source is considered:

$$EER_{\text{unit}} = \frac{E_{\text{unit}}}{E_{\text{total}}} \tag{17}$$

$$EER_{\text{syst}} = \frac{E_{\text{unit}}}{E_{\text{grid}}} \tag{18}$$

The principles of heat and mass transfer between the humid air stream and the water circulating in an evaporative conditioner are described in Kuehn et al. [25]. Typically, parameters such as air temperature drop ($T_{\text{in}}-T_{\text{mid}}$) and evaporative efficiency are used to describe the operation of the evaporative conditioner. The evaporative efficiency is an indication of the potential for evaporative cooling and is dependent on the difference between the wet bulb and dry bulb temperatures of the air, so it can be expressed as follows:

$$\epsilon_{\text{evap}} = \frac{\Delta T_{\text{a}}}{\Delta T_{\text{a,max}}} = \frac{T_{\text{in}} - T_{\text{mid}}}{T_{\text{in}} - T_{\text{wb,amb}}} \tag{19}$$

3.2. Uncertainty analysis

Uncertainty analysis in measurements of key performance parameters of the proposed system is performed based on the analytical description of the measurement model using a top-down approach. The individual sources of uncertainty are then propagated and combined according to the recommendations of GUM-JCGM 100:2008 [26].

Accordingly, the measurement uncertainty in the total energy consumption of the whole system during one day, $u_{E_{total}}$, is the combination of the measurement uncertainties of the calculated values of energy supplied by the grid and by the photovoltaic panels, $u_{E_{\text{grid}}}$ and $u_{E_{\text{pv}}}$, respectively. In other words,

$$u_{E_{\text{total}}} = k\sqrt{u^2_{E_{\text{grid}}} + u^2_{\text{E}_{\text{pv}}} + u^2_{\text{Rie,grid}} + u^2_{\text{Rie,pv}}} \tag{20}$$

where k is the coverage factor for a corresponding level of confidence.

In order to estimate the error committed in the calculation of the variables E_{grid} and E_{pv}, the error of propagation of the uncertainty associated with the current and voltage measurements has been taken into account, together with the error inherent in the Riemann sums expressed by Eqs. (10)–(11).

The uncertainty associated with left or right Riemann sums can be estimated using the following expression,

$$u_{\text{Rie}} \leq \frac{M n \Delta t^2}{\sqrt{12}} \tag{21}$$

where n is the number of current and voltage data points per day over the test duration (14 h), Δt is the time interval (10 s) between two consecutive measurements and M is an upper limit for the derivatives of $\dot{W}_{\text{grid}}$ and $\dot{W}_{\text{pv}}$ over the test duration.

On the other hand, AC and DC voltage (V) and current (I) measurements have been made for the calculation of E_{grid} and E_{pv}, respectively. Since the mean values of V and I have been obtained from simultaneous measurements of both quantities, these variables are correlated and it is necessary to include their correlation coefficient in the evaluation of uncertainties $u_{E_{\text{grid}}}$ and $u_{E_{\text{pv}}}$, that is,

$$u_{E_{\text{grid}}} = \sqrt{n}\Delta t \cos\phi \sqrt{I^2_{\text{ac}} u^2_{V_{\text{ac}}} + V^2_{\text{ac}} u^2_{I_{\text{ac}}} + 2 r_{\text{ac}} V_{\text{ac}} I_{\text{ac}} u_{V_{\text{ac}}} u_{I_{\text{ac}}}} \tag{22}$$

$$u_{E_{\text{pv}}} = \sqrt{n}\Delta t \sqrt{I^2_{\text{dc}} u^2_{V_{\text{dc}}} + V^2_{\text{dc}} u^2_{I_{\text{dc}}} + 2 r_{\text{dc}} V_{\text{dc}} I_{\text{dc}} u_{V_{\text{dc}}} u_{I_{\text{dc}}}} \tag{23}$$

where r is the estimated correlation coefficient between V and I, and $\cos\phi$ is the power factor determined by an experimental correlation from the mains voltage.

With respect to the uncertainties of the direct experimental voltage and intensity measurements, u_V and u_I, they are quantified as the combination of the sources of uncertainty associated with the measurement procedure. Assuming a uniform distribution for the accuracy of the voltage and intensity transducers ($\pm tr_{\text{acc}}$, see Table 2), the standard uncertainty of the measurements can be expressed as,

$$u_{\text{meas}} = \sqrt{u^2_{\text{rd}} + u^2_{\text{tr}} + u^2_{\text{da}}} \tag{24}$$

$$u_{\text{tr}} = \frac{tr_{\text{acc}}}{\sqrt{3}} \tag{25}$$

where the following variables are considered to represent the standard uncertainties associated with the measurements: u_{meas} for the combined uncertainty of measurement; u_{rd} for the repeatability of transducer readings; u_{tr} for the accuracy of the calibrated transducer; u_{da} for the reading accuracy of the data acquisition unit.

Similarly, it is possible to calculate the uncertainty of the remaining performance parameters: solar contribution (SC), energy efficiency ratio of the AC unit (EER_{unit}) and energy efficiency ratio of the whole system (EER_{syst}). Assuming that the individual measurements are uncorrelated and random, the uncertainty in the calculated quantity can be determined as,

$$u_{\text{SC}} = k\sqrt{\left(\frac{u_{E_{\text{pv}}}}{E_{\text{total}}}\right)^2 + \left(\frac{E_{\text{pv}}}{E^2_{\text{total}}} u_{E_{\text{total}}}\right)^2} \tag{26}$$

$$u_{EER_{\text{unit}}} = k\left[\left(\frac{h_1 - h_6}{\dot{W}_{\text{total}}}\right)^2 u^2_{\dot{m}_{\text{ref}}} + \left(\frac{\dot{m}_{\text{ref}}}{\dot{W}_{\text{total}}}\right)^2 \left(u^2_{h_1} + u^2_{h_2}\right) + \left(\frac{\dot{m}_{\text{ref}}(h_1 - h_6)}{\dot{W}^2_{\text{total}}}\right)^2 \left(u^2_{\dot{W}_{\text{grid}}} + u^2_{\dot{W}_{\text{pv}}}\right)\right]^{1/2} \tag{27}$$

$$u_{EER_{\text{syst}}} = k\sqrt{\left(\frac{u_{EER_{\text{unit}}}}{1 - SC}\right)^2 + \left(\frac{EER_{\text{unit}}}{(1 - SC)^2} u_{SC}\right)^2} \tag{28}$$

where $u_{\dot{m}_{\text{ref}}}$, u_{h_1} and u_{h_2} are calculated from the uncertainties in the temperature and pressure measurements of the refrigeration cycle, according to Eqs. (24)–(25), and using the uncertainty propagation tool of the Engineering Equation Solver (EES) software; $u_{\dot{W}_{\text{grid}}}$ and $u_{\dot{W}_{\text{pv}}}$ are calculated by dividing Eq. (22) by $\sqrt{n}\Delta t$.

According to this uncertainty analysis and considering a coverage factor $k = 2$, corresponding to a confidence level of about 95 %, the maximum relative expanded uncertainties have been obtained for the following performance parameters: $u_{E_{\text{total}}} \leq 0.8\,\%$, $u_{SC} \leq 1.5\,\%$, $u_{EER_{\text{unit}}} \leq 4.1\,\%$ and $u_{EER_{\text{syst}}} \leq 4.2\,\%$.

Finally, it was found that the main source of uncertainty for the calculation method used in this study is related to the accuracy of the AC voltage and current transducers (MCR-VAC-UI-O-DC and MCR-S-1/5-UI-DCI-NC respectively). Therefore, if there is a need to reduce the uncertainty of the values obtained for the key performance parameters of the system, it will first be necessary to find an alternative for this instrumentation.

On the other hand, if instead of calculating the refrigerant mass flow rate ($\dot{m}_{\text{ref}}$), we decide to purchase a Coriolis mass flow meter to perform these measurements with a relative uncertainty of 0.2 % [27], the new maximum relative expanded uncertainties for the energy efficiency ratios will be: $u_{EER_{\text{unit}}} \leq 2.2\,\%$ and $u_{EER_{\text{syst}}} \leq 2.3\,\%$.

4. Experimental results

4.1. Results of daily measurements

This section shows two sets of measurements, both with pre-cooling (mode 2) and without pre-cooling (mode 1) applied to the air conditioning system on two different days, to illustrate the operation of the laboratory prototype. These two days were chosen to ensure that the environmental conditions were as similar as possible. To describe the environmental conditions, Fig. 5 shows the results of the irradiance recorded on 13 and 21 August. As can be seen, both days were quite

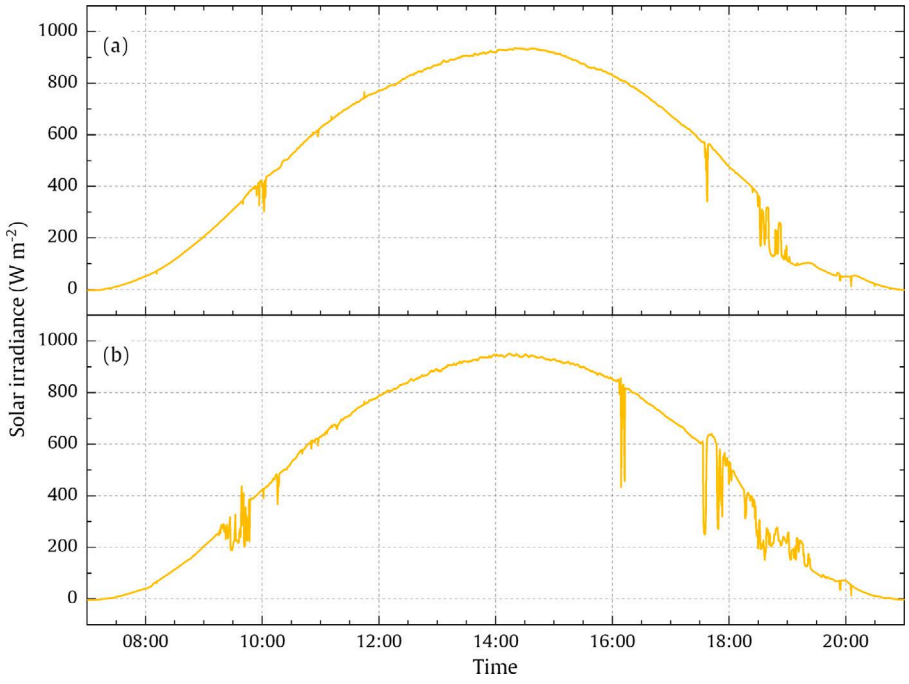

Fig. 5. Measurements of solar irradiance: (a) on 13 August with air conditioning system operating in mode 1, (b) on 21 August with air conditioning in mode 2 with pre-cooling.

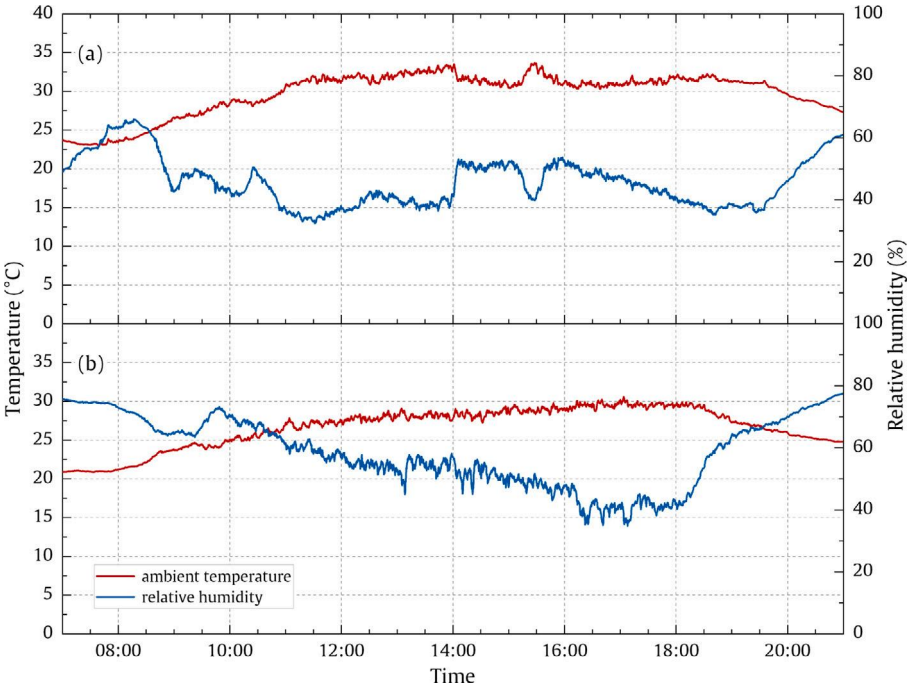

Fig. 6. Ambient air temperature and relative humidity measurements: (a) on 13 August with air conditioning system operating in mode 1, (b) on 21 August with air conditioning in mode 2 with pre-cooling.

similar and completely clear, with irradiance above 900 W m^{-2} at mid-day and total available solar energy of 6964 Wh d^{-1} and 7071 Wh d^{-1} respectively.

Dry ambient temperature and relative humidity also followed a similar trend, see Fig. 6.

To describe the evolution of the air in the condenser in mode 1, Fig. 7(a) shows the sensible heating of the air as it passes through the heat exchanger. As there is no pre-cooling, the measurements at the inlet and intermediate points (after the pad) are in agreement, except for the uncertainty of the sensors. In mode 2, see Fig. 7(b), the air passing through the evaporative section is cooled from approximately 30 °C to 25 °C. It should be noted that when the pre-cooling is active, the relative humidity at the intermediate point is above 80 %.

Both processes are plotted on a psychrometric diagram which clearly shows the almost isenthalpic evolution of the air in the evaporative section and the horizontal evolution of the psychrometric heat transfer process as it passes through the heat exchanger. As expected with the use of pre-cooling, Fig. 8 shows a significant drop in the temperature of the air entering the condenser. The outlet conditions should remain in the same horizontal plane as those corresponding

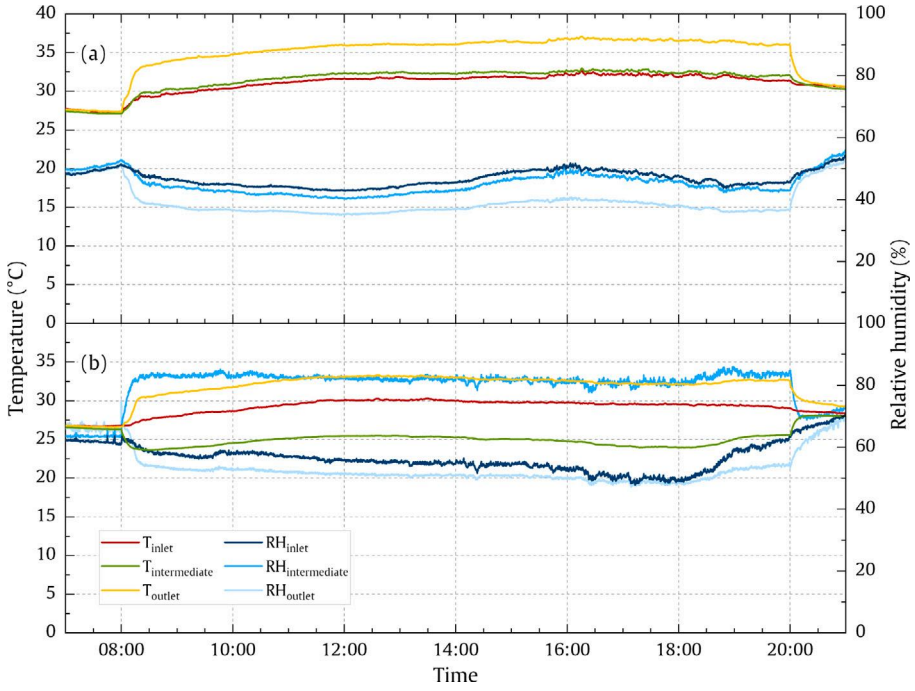

Fig. 7. Air temperature and relative humidity measurements at the inlet, intermediate and outlet sections: (a) on 13 August with air conditioning system operating in mode 1, (b) on 21 August with air conditioning in mode 2 with pre-cooling.

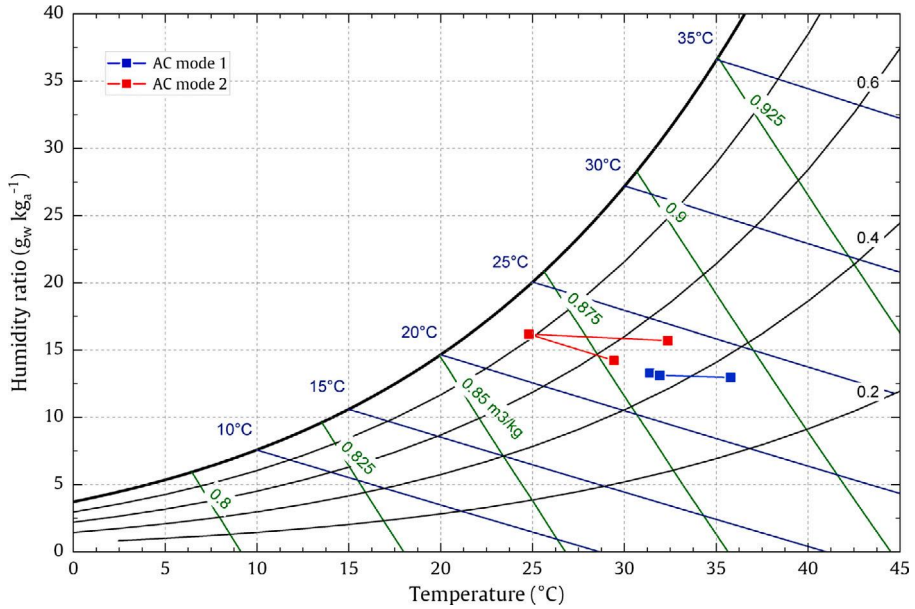

Fig. 8. Air psychrometric processes in the condenser: (blue) on 13 August with air conditioning system operating in mode 1, (red) on 21 August with air conditioning in mode 2 with pre-cooling.

to the intermediate point. However, the observed drop is due to the mixing of the outlet air with the ambient air.

When analysing what happens in the evaporative section, the greater difference between the wet bulb temperature and the ambient temperature, which causes greater cooling, is found in the afternoon, reaching values above 5 °C. However, as described in the literature, evaporative efficiency is independent of ambient conditions [28–30]. Since the AC unit operates at a load factor of 100 %, the volumetric air flow through the condenser is maintained at a constant value of 1860 $m^3\,h^{-1}$ and the average air velocity through both the condenser and the evaporative pads reaches an average value of approximately 1.3 $m\,s^{-1}$. Under these conditions, the evaporative efficiency remains relatively stable throughout the day, see Fig. 9, with values in the range of about 60 % to 70 %. The average evaporative efficiency for all tests performed in this study was $\varepsilon_{evap} = 67.4\,\%$.

The effect of pre-cooling the condenser air inlet temperature is reflected in the thermal performance of the refrigerant inside the unit. Fig. 10 shows the temperature and pressure of the refrigerant throughout the refrigeration cycle. In Fig. 10(a) it can be seen that the temperature at the compressor outlet is higher than 90 °C when pre-cooling is not activated (mode 1). Conversely, Fig. 10(b) shows that this temperature does not reach 80 °C when pre-cooling is activated (mode 2). The same applies to the pressure values of the refrigerant cycle and Fig. 10(c) shows a condensation pressure of more than 25 bar for the

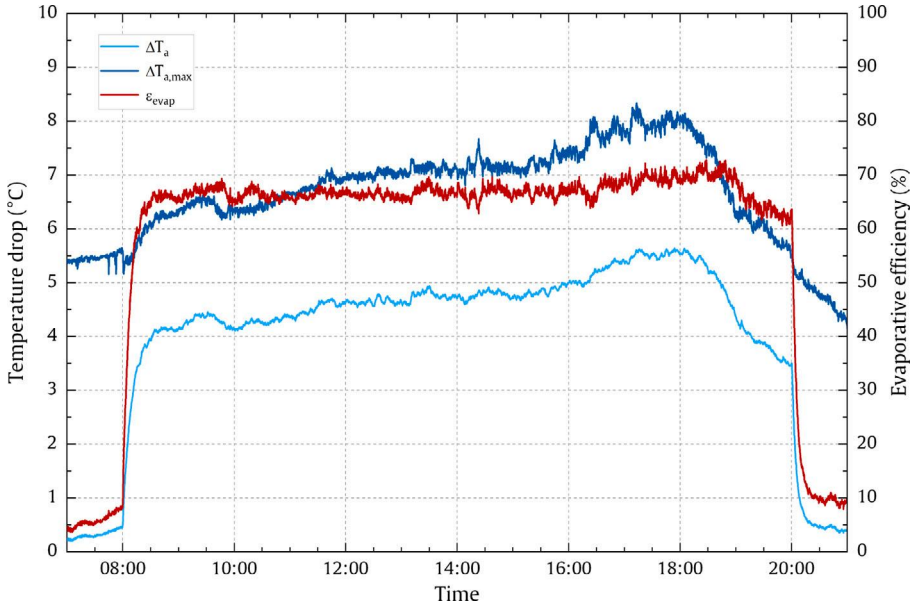

Fig. 9. Air temperature drop and evaporative cooling efficiency recorded on 21 August with air conditioning system operating in mode 2.

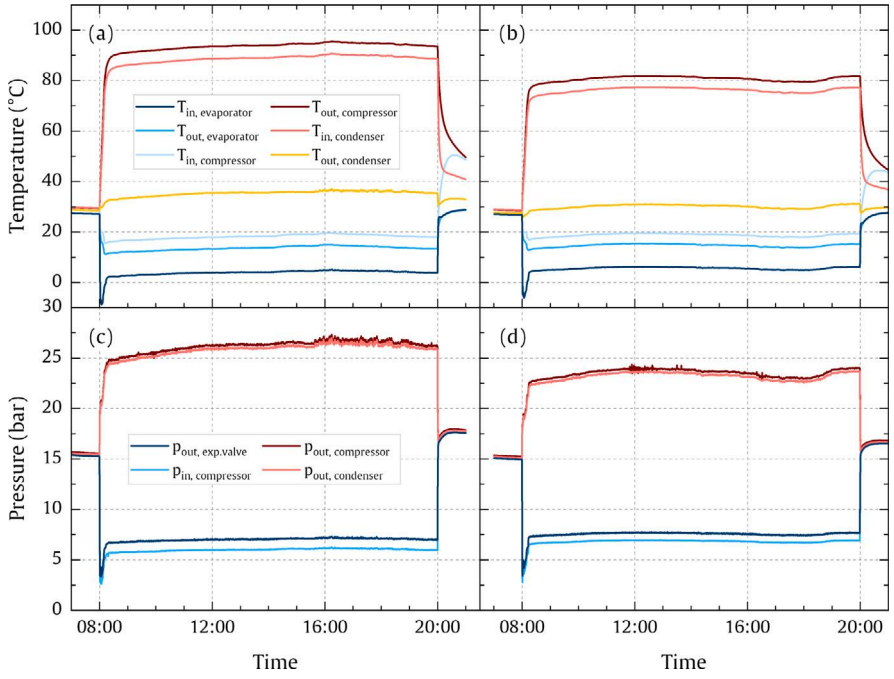

Fig. 10. Development of refrigerant temperature and pressure: (a, c) on 13 August with air conditioning system operating in mode 1, (b, d) on 21 August with air conditioning in mode 2 with pre-cooling.

entire operating time of the system without pre-cooling (mode 1) and in Fig. 10(d) this value is reduced to levels below 23 bar with pre-cooling (mode 2).

Fig. 11 presents the Mollier (p-h) diagram showing the changes in the refrigerant cycle between the two days being compared. A clear difference between the operating conditions of the refrigerant with and without evaporative pre-cooling can be seen in this figure.

Fig. 12 shows, superimposed on the solar irradiance, the most descriptive electrical power values of the system operation: the total power consumed by the system, the power required from the grid and the power coming from the PV modules. The management carried out by the equipment between grid consumption and photovoltaic production can be checked on the graph. The total electrical power consumed by the air conditioning system in mode 1 is greater than 1000 W (peak power of 1138 W) in the middle hours of the day. In this period of the day, the peak power of the PV modules is 371 W, which implies a module efficiency of between 11–12 %, and the grid power is 746 W. The peak power consumed by the grid is 1035 W, which occurs between 7.00 pm and 8.00 pm, when the solar contribution is negligible. In terms of daily energy, the total energy consumed by the system is 13.1 kWh d^{-1}, the energy consumed from the grid is 10.2 kWh d^{-1} and the energy provided by the PV modules is 2.9 kWh d^{-1}. This gives a solar contribution (*SC*) of 22 %.

With evaporative pre-cooling activated for the condenser (mode 2), there is a significant reduction in both peak power and daily energy consumption. The total peak power consumed in this second test is

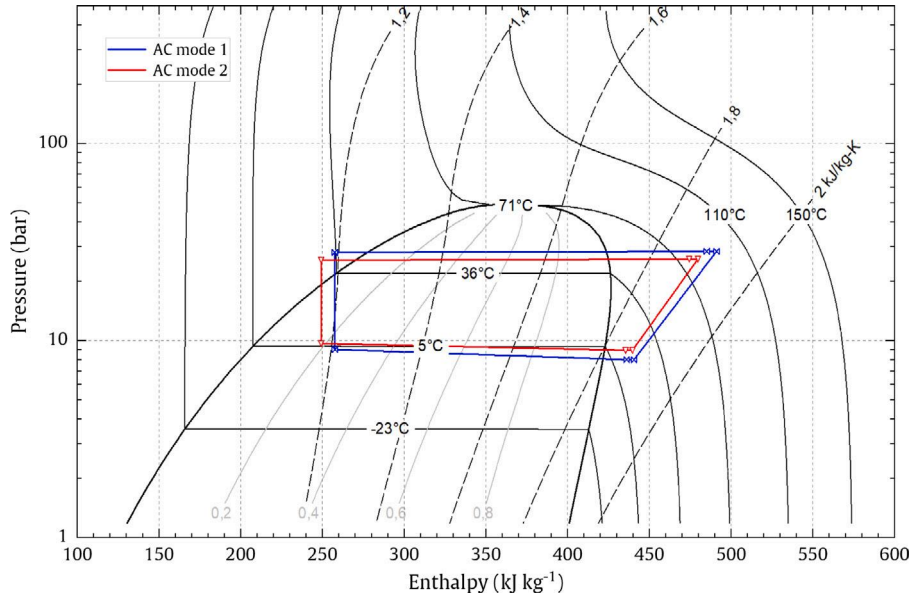

Fig. 11. R410A pressure enthalpy chart (p-h): (blue) on 13 August with air conditioning system operating in mode 1, (red) on 21 August with air conditioning in mode 2 with pre-cooling.

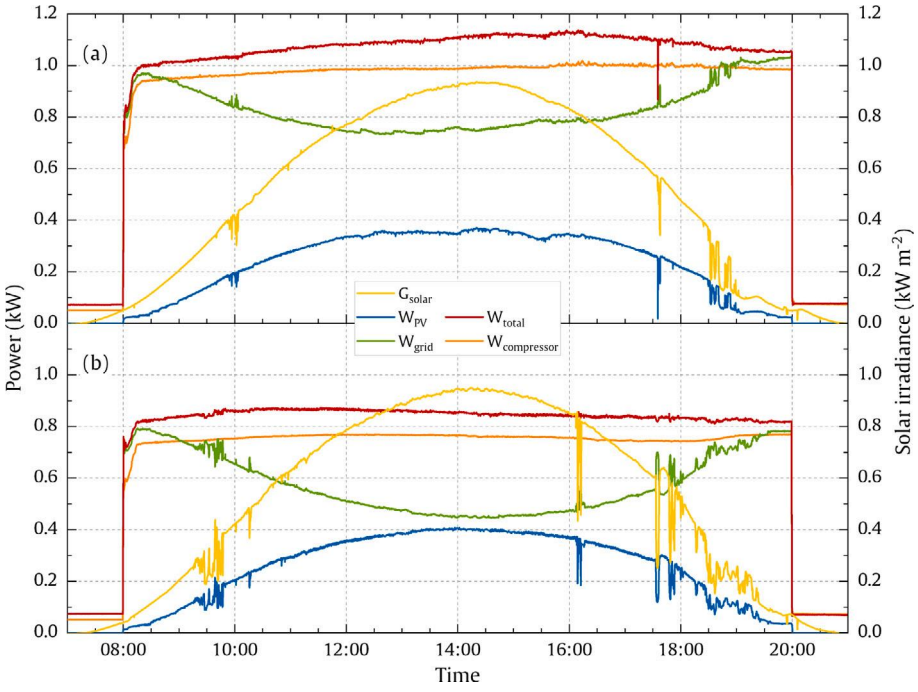

Fig. 12. Solar irradiance and electrical power exchanged in the air conditioning system.: (a) on 13 August with air conditioning system operating in mode 1, (b) on 21 August with air conditioning in mode 2 with pre-cooling.

874 W and the peak grid power is 793 W, a reduction of 23 % in both cases. In terms of daily energy, the total energy consumed by the system is 10.3 kWh d^{-1}, the energy consumed from the grid is 7.1 kWh d^{-1} and the energy provided by the PV modules is 3.1 kWh d^{-1}. With these data, a reduction in total energy consumption of 3.0 kWh d^{-1} (29.7 %) is achieved. The average daily solar contribution rises to 31 % and exceeds 47 % at midday.

From the set of measurements, the overall performance of the baseline air conditioning system with air-cooled condenser (mode 1) and the performance of the proposed system with evaporative-cooled condenser (mode 2) were determined in terms of cooling capacity and power supplied. The energy efficiency of the air conditioning unit was calculated using Eq. (17) and the energy efficiency of the whole system (AC unit + photovoltaic) is calculated by counting only the energy consumed from the grid, Eq. (18). From the values shown in Fig. 13, the average daily energy efficiency of the unit operating in mode 1 was $EER_{unit} = 3.96$ and the energy efficiency achieved in mode 2 with pre-cooling was $EER_{unit} = 4.67$. This difference in energy efficiency becomes even greater when the EER_{syst} of the whole system is calculated for the two operating modes: an average daily value of $EER_{syst} = 5.18$ was obtained in mode 1 compared to $EER_{syst} = 7.04$ in the case of the condenser with pre-cooling, reaching values of $EER_{syst} > 8.7$ at midday.

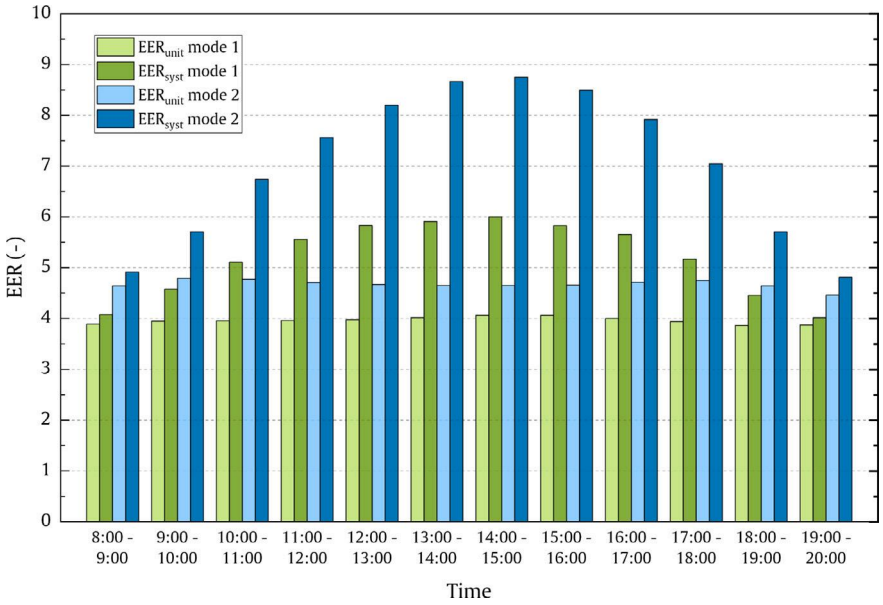

Fig. 13. Energy efficiency of the AC unit and energy efficiency of the whole system (AC unit + PV): on 13 August with air conditioning system operating in mode 1, and on 21 August with air conditioning in mode 2 with pre-cooling.

Table 3
Measurement of the psychrometric conditions in the evaporative pre-cooling section and calculation of the water consumption of the system on 21 August with air conditioning in mode 2.

Time	T_{amb} °C	RH_{amb} %	T_{mid} °C	RH_{mid} %	$T_{wb,amb}$ °C	ω_{amb} $kg_w\ kg_a^{-1}$	ω_{mid} $kg_w\ kg_a^{-1}$	ε_{evap} %	$\dot{V}_{w,evap}$ $L\,h^{-1}$	$\dot{V}_{w,supply}$ $L\,h^{-1}$
8 h–9 h	27.5	59.4	24.0	81.2	21.6	0.0137	0.0152	59.8	3.3	4.1
9 h–10 h	28.5	57.5	24.2	83.3	22.0	0.0140	0.0158	66.9	3.9	4.8
10 h–11 h	29.1	57.8	24.9	83.2	22.7	0.0147	0.0165	66.2	3.9	4.8
11 h–12 h	29.9	56.3	25.3	82.5	23.1	0.0149	0.0168	66.4	4.2	5.0
12 h–13 h	30.1	55.5	25.5	82.1	23.1	0.0149	0.0169	66.3	4.3	5.1
13 h–14 h	30.1	54.9	25.4	82.0	23.0	0.0148	0.0168	66.8	4.4	5.2
14 h–15 h	29.9	54.4	25.1	81.7	22.7	0.0144	0.0164	66.6	4.4	5.2
15 h–16 h	29.8	53.9	25.0	81.5	22.5	0.0142	0.0162	66.7	4.4	5.3
16 h–17 h	29.7	51.4	24.5	80.7	22.0	0.0134	0.0156	67.5	4.7	5.6
17 h–18 h	29.6	49.7	24.1	80.8	21.6	0.0129	0.0152	69.2	5.0	5.9
18 h–19 h	29.5	52.8	24.3	82.8	22.1	0.0137	0.0158	70.1	4.7	5.6
19 h–20 h	29.3	60.6	25.4	83.7	23.3	0.0156	0.0172	64.2	3.5	4.4
Average	29.4	55.3	24.8	82.1	22.5	0.0143	0.0162	66.4	4.2	5.1

4.2. Water consumption

In Section 2.2, an initial estimate of $9.6\,L\,h^{-1}$ for the water consumption of the evaporative pre-cooling system was calculated from Eq. (3), based on the technical specifications provided by the pad manufacturer. In this section, the actual average water consumption is calculated using Eqs. (3) and (4), and the measurements taken on the prototype.

Table 3 shows the measurements obtained during the test on 21 August with the air conditioner in mode 2, and the hourly evolution of the system's water consumption. The average hourly consumption for this day was $\dot{V}_{w,supply,21Aug} = 5.1\,L\,h^{-1}$.

As can be seen from this table, the actual water consumption was much lower than previously estimated, mainly due to the fact that the actual evaporative efficiency of the panels was also much lower than the efficiency given in the technical specifications. The air conditioning system consumed a total of 60.8 L during its 12 h of operation. Finally, the average water consumption calculated over all the tests carried out in similar environmental conditions was $\dot{V}_{w,supply,avg} = 5.1\,L\,h^{-1}$, with a range of variation between 4.5 and $5.9\,L\,h^{-1}$.

Although the daily water consumption may seem high at first glance, it is important to note that all tests were carried out with the air conditioner in continuous operation, with a load factor of $LF = 100\,\%$. Therefore, this consumption represents the maximum possible for the given environmental conditions. Under normal air conditioner operating conditions, a 40 to 60 % reduction in water consumption can be expected. This water consumption can be further reduced if it is possible to use the condensation water produced by the air conditioning system, which can represent an additional saving on average of up to 20 % of the system's water consumption and up to 35 % on days when the ambient relative humidity is above 65 %.

Daily water consumption is variable and depends mainly on the ambient operating conditions of the system. Fig. 14 shows the estimated maximum consumption of the air conditioning system operating in mode 2 at 100 % load factor, for the expected range of ambient temperatures and relative humidities.

4.3. Results for different environmental conditions

This section presents the results of a series of tests carried out with the air conditioning system operating in modes 1 and 2, under different environmental conditions during a typical Mediterranean summer. In order to assess the possible negative effect of the presence of the cooling pads at the condenser inlet when not in use, the results have also included the tests corresponding to the air conditioning system operating in mode 3. As indicated in Section 2.4, in mode 3 the cooling

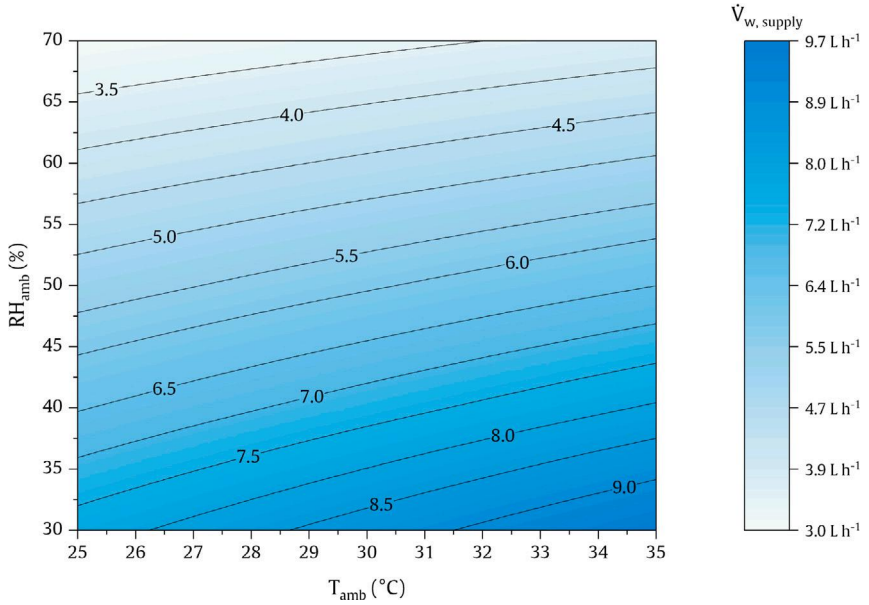

Fig. 14. Estimated maximum water consumption, $\dot{V}_{w,supply}$, of the air conditioner in mode 2, depending on the ambient conditions in terms of temperature and relative humidity.

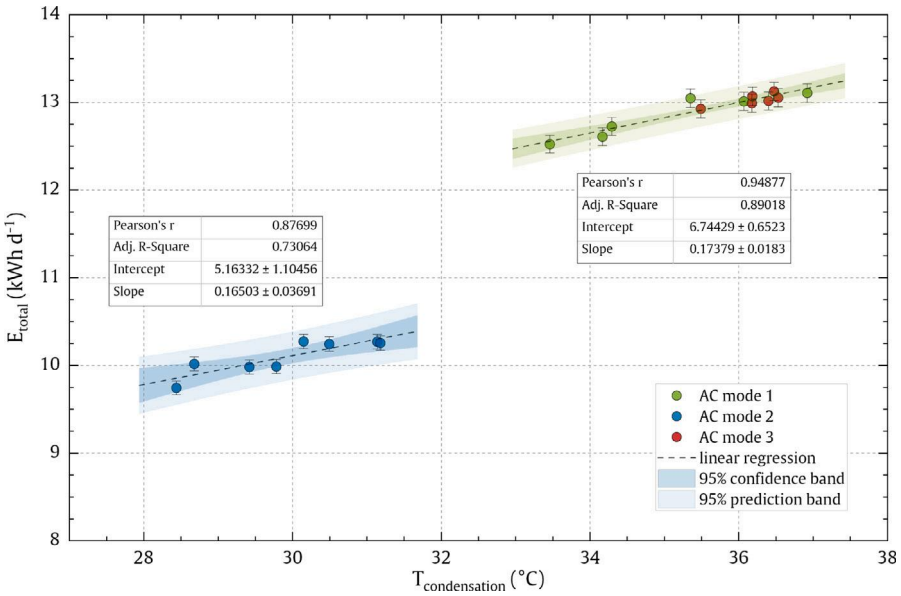

Fig. 15. Total daily energy consumption of the AC system as a function of air condensation temperature and different operating modes during a typical Mediterranean summer.

pads are installed and the water recirculation is deactivated, so there is no pre-cooling, but the pads continue to cause a pressure drop in the air flow through the condenser.

In Fig. 15, the total energy consumption of the system over the course of a day is plotted against the air condensation temperature. Each point represents the integral or average value from 8.00 am to 8.00 pm for each test day. It can be seen that the tests carried out with pre-cooling (mode 2) have a lower condensation temperature and, as expected, the daily energy consumption is lower. On average, the total daily energy consumption for the days in which the system operated in mode 1 is 12.8 kWh d^{-1} and in mode 3 is 13.1 kWh d^{-1}, which shows a fairly similar behaviour. In mode 2, the fact that the air condensation temperature is reduced by pre-cooling makes it possible to reduce the total daily energy consumption to 10.1 kWh d^{-1}, as can be seen from the graph in Fig. 15, and the average daily grid energy consumption to 7.3 kWh d^{-1}. A standard AC unit without PV input or evaporative pre-cooling would have drawn 12.8 kWh d^{-1} of energy from the grid, so these two improvements represent an average 43 % reduction in energy consumption.

Fig. 16 shows the daily energy drawn from the grid by the AC system against the solar radiation. The test was carried out on mostly clear days, but data for cloudy days is also included. It can be seen that the more solar energy is available, the less energy is drawn from the grid. It can also be seen that the consumption of non-renewable energy is significantly lower in the pre-cooling mode, with a reduction of around 2.7 kWh d^{-1}. Fig. 16 also shows the minor negative impact when the pads are permanently installed but not in use (mode 3) by causing a pressure drop in the air flow through the condenser and a grid power consumption slightly higher than the consumption in mode 1. However, the magnitude of this negative impact does not seem to justify the work involved in removing the panels when the air conditioning system is operating in heating mode during the winter season.

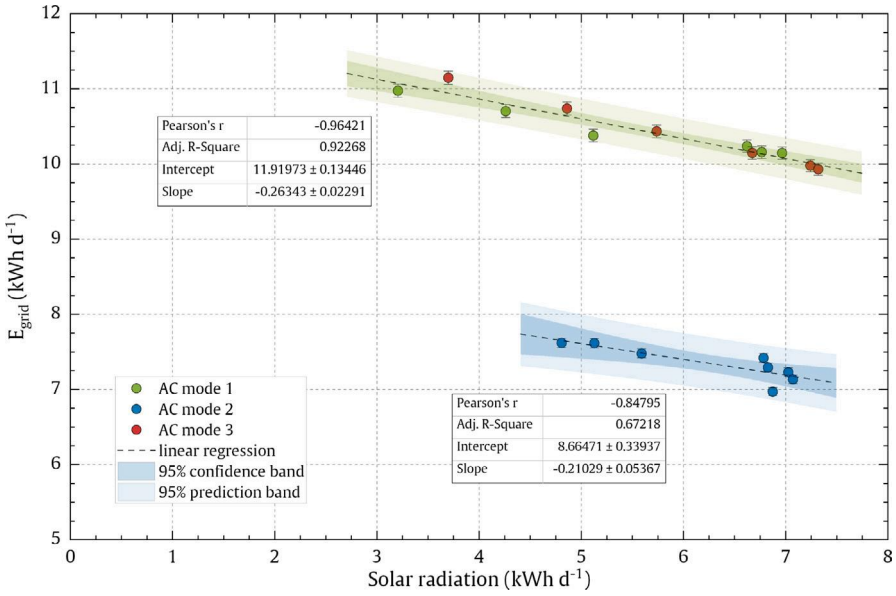

Fig. 16. Daily energy drawn from the grid by the AC system as a function of solar radiation and different operating modes during a typical Mediterranean summer.

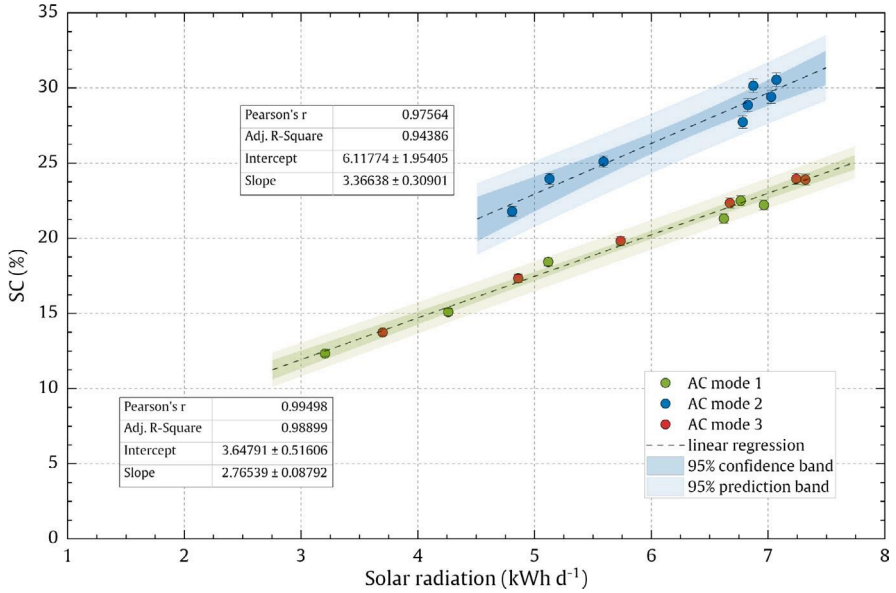

Fig. 17. Solar contribution as a function of daily solar radiation during a typical Mediterranean summer. Performance comparison of different AC operating modes.

Regarding the solar contribution (*SC*) in the AC system under different irradiation conditions, Fig. 17 shows that solar contribution values of more than 30 % are achieved when pre-cooling is used on clear days. This is in contrast to operating the system under standard operating conditions without pre-cooling, where only 25 % solar contribution is achieved. On average, the solar contribution in mode 2 is 45 % higher than in modes 1 and 3.

The effect of reducing the condensing temperature on the refrigeration cycle is shown in Fig. 18. The EES software [24] was used to calculate the thermodynamic properties of R410A refrigerant based on the assumptions described in the methodology Section 2. The graph shows the significant improvement in the energy efficiency ratio of the AC unit (EER_{unit}) when the pre-cooling is activated.

In Fig. 18, a sub-graph has been added to show the effect of variations in ambient conditions on the efficiency of the AC unit operating in mode 2. The variations of T_{amb} and RH_{amb} can be considered together by calculating the variable $\Delta T_{a,max}$. The sub-graph shows that, for example, if we consider constant ambient temperature conditions, a decrease in ambient relative humidity causes an increase in $\Delta T_{a,max}$ and therefore an increase in the capacity of the evaporative pre-cooling system to cool the air flowing through it, which ultimately translates into an increase in the efficiency of the air conditioner.

Considering only the non-renewable energy consumption, the energy efficiency ratio of the system (EER_{syst}) can be calculated by taking into account the EER_{unit} and the solar contribution. Fig. 19 shows the energy efficiency ratio of the system as a function of the solar contribution for several daily tests carried out during a typical Mediterranean summer. To confirm the measurement procedure, the graph also includes experimental data from a similar study carried out by Aguilar et al. [5]. The agreement between the experimental data obtained in this study and the previously published data by Aguilar et al. [5] is evident, despite the fact that these authors carried out their tests on a different type of building, with different environmental and operating conditions and with a different number of PV modules.

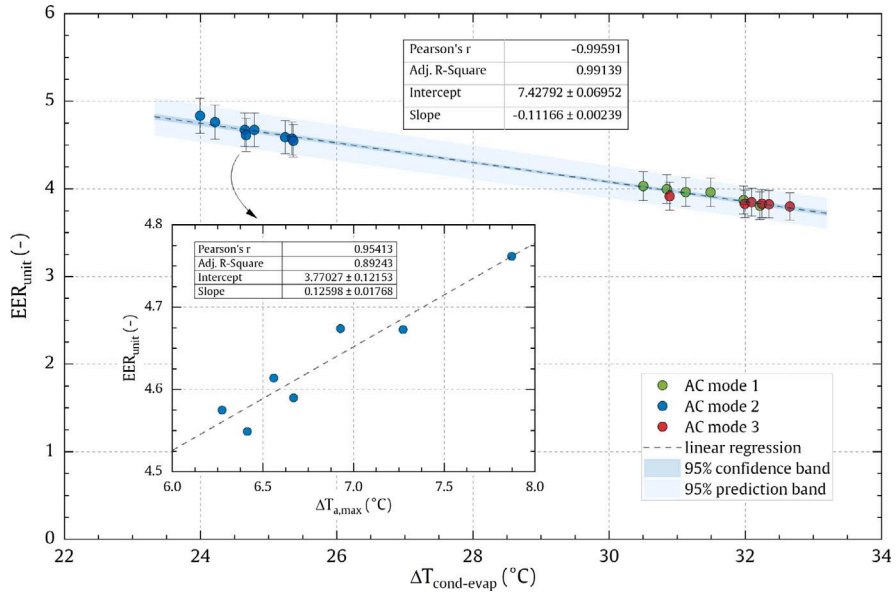

Fig. 18. Energy efficiency ratio of the unit as a function of the temperature difference between the evaporator and condenser during a typical Mediterranean summer. Performance comparison of different AC operating modes.

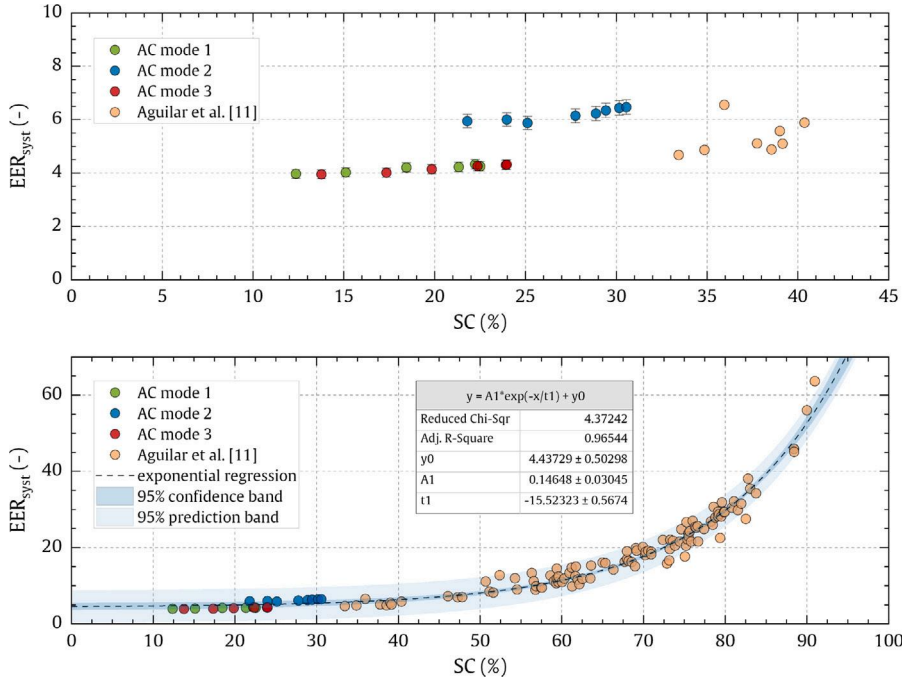

Fig. 19. Energy efficiency ratio of the system as a function of solar contribution during a typical Mediterranean summer. Performance comparison of different AC operating modes.

The results in Fig. 19 show that the evaporative pre-cooling mode provides the highest EER_{syst} values for a given solar contribution, with values ranging from 5.9 to 6.5 in mode 2, with an average value of $EER_{syst} = 6.17$. Compared to AC mode 1, the graph also shows that with pre-cooling enabled, there is a significant improvement in the energy efficiency ratio of the system, increasing the average EER_{system} from 4.16 to 6.17.

4.4. Techno-economic analysis

This section presents a brief techno-economic analysis to evaluate the energy savings and environmental impact of using solar energy and evaporative pre-cooling when the proposed air conditioning system operates in modes 1 and 2, compared to a standard air-conditioning system without PV input.

To carry out this analysis, experimental data on heating and cooling energy demand collected by the authors over a whole year in a 35 m^2 office located on the second floor of an office building in southeastern Spain were used [5]. The indoor unit was placed inside the office, while the outdoor unit was installed on the roof of the building. Typical occupancy profiles were observed as during office hours, from 8.00 am to 8.00 pm. The simulation of the behaviour of the proposed system takes into account that the air conditioning system operates in heating mode from November to April, powered simultaneously by the grid and the PV panels, and in cooling mode (in operation modes 1 and 2) from May to October. The air conditioning control has been configured

Table 4
Techno-economic analysis and performance statistics over one year of simulated operation of the air conditioning system in an office space located in southeastern Spain.

	Reference AC[a]	Standard AC[b]	AC mode 1	AC mode 2
Energy savings				
Annual energy balance ($kWh\,yr^{-1}$)				
Thermal energy supplied, $\Sigma_i E_{unit,i}$	6523	6523	6523	6523
Grid energy consumption, $\Sigma_i E_{grid,i}$	2609	1470	679	625
EER_{syst} (–)	2.50	4.44	9.61	10.44
SC (%)	–	–	53.8	55.9
Environmental impact				
Primary non-renewable energy ($kWh\,yr^{-1}$)	5236	2950	1362	1254
CO_2 emissions ($kg\,yr^{-1}$)	931	525	242	223
Economic analysis				
Capital investment costs (€)				
PV panels (750 Wp total)	–	–	272.00	272.00
Support for PV panels	–	–	215.00	215.00
Air Conditioner	850.00	1315.00	1315.00	1315.00
Evaporative pads	–	–	–	50.00
Pump system	–	–	–	55.00
Design/planning/other costs	200.00	200.00	200.00	200.00
General installation costs	300.00	500.00	760.00	800.00
Indirect costs	75.00	125.00	190.00	200.00
total	1425.00	2140.00	2952.00	3107.00
Annualised replacement costs ($€\,yr^{-1}$)				
PV panels (25 yr lifetime)	–	–	–	–
Air Conditioner (18 yr lifetime)	11.15	17.25	17.25	17.25
Evaporative pads (6 yr lifetime)	–	–	–	7.75
total	11.15	17.25	17.25	25.00
Maintenance ($€\,yr^{-1}$)				
PV panels	–	–	30.00	30.00
Air conditioner	60.00	60.00	60.00	60.00
total	60.00	60.00	90.00	90.00
Operating costs ($€\,yr^{-1}$)				
Electricity consumption cost	386.13	217.52	100.46	92.44
Electricity capacity cost	90.00	90.00	90.00	90.00
Water consumption				4.71
total	476.13	307.52	190.46	187.15
Annualised costs ($€\,yr^{-1}$)				
Investment	79.45	119.32	164.59	173.23
Replacement	11.15	17.25	17.25	25.00
Maintenance	60.00	60.00	90.00	90.00
Operation	476.13	307.52	190.46	187.15
total	626.73	504.08	462.30	475.38
Financial metrics				
CR (–)	ref.	0.80	0.74	0.76
(cost ratio)		ref.	0.92	0.94
Payback (yr)	ref.	4.61	6.68	7.54
(discounted payback period)		ref.	11.11	14.40
SIR (–)	ref.	2.96	1.85	1.55
(discounted savings to investment ratio)		ref.	0.87	0.54
NPV (€)	ref.	2114.92	2818.79	2611.07
(net present value)		ref.	703.87	525.52
Reference costs and energy factors				
Consumption-based costs				
Electricity (energy costs)[c]	$0.148\ €\,kWh^{-1}$			
Electricity (power costs)	$90\ €\,yr^{-1}$			
Water	$1.90\ €\,m^{-3}$			
Economic-based costs				
Period under consideration	25 yr			
Inflation rate	3 %			
Market discount rate	3 %			
Energy conversion factors [31]				
primary non-renewable energy ($kWh_p\,kWh_e^{-1}$)	2.007			
Emissions factor ($kg_{CO_2}\,kWh_e^{-1}$)	0.357			

[a] Low price/performance air conditioner used as a benchmark.
[b] Standard air conditioner model without photovoltaic energy input.
[c] Average price of the PVPC regulated tariff in Spain in 2023.

to meet the thermal needs of the office space under normal activity and occupancy conditions. For the purposes of the study, the indoor thermostat temperature was set at 23 °C in cooling mode and 21 °C in heating mode.

Table 4 shows the results of the system performance simulation over one year of operation, maintaining the comfort conditions of the reference air-conditioned office. In order to simulate the behaviour of the air conditioning system, the correlations previously obtained were taken into account to calculate the EER_{unit} and EER_{syst} in modes 1 and 2, depending on the operating parameters of the system and the environmental and solar radiation conditions. The following correlation has also been taken into account to estimate the EER_{unit} value when the air conditioner is operating at partial loads:

$$EER_{unit} = 5.7055 - 0.0474\Delta T_{mid} + 4.3236LF - 0.0009\Delta T_{mid}LF - 7.1835LF^2 \quad (29)$$

where LF is the load factor and ΔT_{mid} is a centred value of T_{mid} with respect to a reference temperature of 25 °C.

In order to assess the environmental and economic feasibility of the proposed system, four different system configurations are studied, as shown in Table 4: reference AC, standard AC, AC mode 1 and AC mode 2. The reference AC is a low cost/performance air conditioner used as a benchmark, consisting of a reversible air conditioner for heating and cooling, which is a very common solution for space cooling/heating of buildings in the Mediterranean region. The unit is considered to have a seasonal efficiency of 2.5. The standard AC and AC modes 1 and 2 consist of the same high-efficiency AC model unit running in three different operating modes, where in standard mode the air conditioner operates without photovoltaic energy input or evaporative pre-cooling in the condenser.

The results of the performance simulation of the AC system shown in Table 4 indicate that, from the point of view of the environmental impact of the system, when the AC system operates in modes 1 and 2, a significant reduction in primary energy consumption and greenhouse gas emissions is achieved, thus benefiting the environment. When operating in mode 2, the system achieves an 8.0 % reduction in primary energy consumption and CO_2 emissions compared to mode 1, and a 57.5 % reduction compared to the standard AC unit. Compared to the reference AC unit, the reduction in primary energy and CO_2 emissions in mode 2 is up to 76.1 %.

On the other hand, for the economic feasibility study, two scenarios were considered to assess the profitability of modifications to the base air conditioning system. In the first scenario, the reference AC unit was used as a benchmark and in the second, the standard AC unit was used for this purpose. Four financial indicators were calculated to assess the feasibility of the modifications made: cost ratio (CR) or ratio between the total annualised cost of the analysed system and the reference system for the same heating and cooling supply, discounted payback period, discounted savings to investment ratio (SIR) and net present value (NPV).

The economic results in Table 4 show that even with electricity prices as low as those reported for 2023 in Spain, with an average value of only 0.148 € kWh^{-1}, operating modes 1 and 2 are acceptably cost-effective compared to the standard AC unit. A cost ratio of 0.76 and 0.94 of the AC operating in mode 2 compared to the reference AC and standard AC, respectively, indicates that the on-grid hybrid solar air conditioner with evaporative pre-cooling is less expensive than the business-as-usual systems over its entire lifetime. Discounted payback periods of 11.1 and 14.4 years were obtained for modes 1 and 2 respectively. The payback period changes drastically when the electricity price increases and, for example, at a value of 0.30 € kWh^{-1}, the payback period is reduced to only 4.2 and 4.8 years for modes 1 and 2 respectively. As can be seen from the results of this case simulation, for the reference electricity price used in the calculations, mode 2 has no economic advantage over mode 1, with NPVs of 704 € and 526 € associated with the investments needed to operate in modes 1 and 2 respectively. However, at a price of 0.34 € kWh^{-1}, modes 1 and 2 are equally profitable, with a high NPV of 3350 €, and at this price mode 2 starts to be more profitable than mode 1. Furthermore, in this annual comparison, it should be noted that mode 2 is only active for half of the year, from May to October, so it will generally be a much more advantageous option for air conditioners that only meet cooling demand.

5. Conclusions

Experimental tests have been carried out to investigate the thermal and electrical improvement of a grid-connected hybrid solar air conditioning system when using an evaporative pad pre-cooling system at the condenser unit. The results of two days of similar test conditions comparing the effect of evaporative cooling activation were analysed from an energy point of view. A series of daily data collected during the summer in a Mediterranean climate were also compared from an energy point of view. The main conclusions are:

- It has been found that with a 100 mm-thick evaporative pad, an evaporative cooling efficiency (ε_{evap}) of between 60 % and 70 % can be achieved, with an average evaporative efficiency for all tests performed in this study of $\varepsilon_{evap} = 67.4\,\%$, resulting in a drop in inlet air temperature of around 6 °C at midday. This improvement in the condenser inlet air allows the high pressure of the refrigerant circuit to be reduced by approximately 2 bar, resulting in a 18.3 % improvement in the energy efficiency ratio (EER_{unit}) of the AC unit.
- By activating the evaporative pre-cooling of the air flow through the condenser (mode 2), a significant reduction in peak power consumption is observed. The total peak power consumption in these operating conditions is 874 W and the peak grid power consumption is 793 W, a reduction of 23 % in both cases.
- The solar contribution achieved by the system for different irradiation conditions with pre-cooling exceeds 30 % on clear days. However, the solar contribution of the air conditioning system with a standard condenser without pre-cooling is only 25 %.
- From a daily energy point of view, the total energy and grid energy consumed by the air conditioning system was measured, taking into account the photovoltaic contribution. Although the photovoltaic contribution and the improvement in the energy efficiency of the air conditioning system due to the evaporative pre-cooling provide independent benefits, together they result in a maximum reduction in total average daily energy consumption from 12.8 kWh d^{-1} to 7.3 kWh d^{-1}, which represents a 43 % reduction in energy consumption.

CRediT authorship contribution statement

P. Martínez: Conceptualization, Data curation, Formal analysis, Investigation, Methodology, Software, Validation, Visualization, Writing – original draft, Writing – review & editing. **M. Lucas:** Conceptualization, Data curation, Formal analysis, Funding acquisition, Investigation, Methodology, Project administration, Resources, Software, Supervision, Validation, Writing – original draft, Writing – review & editing. **F.J. Aguilar:** Conceptualization, Data curation, Methodology, Resources, Validation, Writing – review & editing. **J. Ruiz:** Conceptualization, Data curation, Methodology, Resources, Software, Validation, Writing – review & editing. **P.V. Quiles:** Conceptualization, Methodology, Resources, Validation, Writing – review & editing.

Declaration of competing interest

The authors declare that they have no known competing financial interests or personal relationships that could have appeared to influence the work reported in this paper.

Data availability

Data will be made available on request.

Acknowledgements

This publication is part of the R+D+i project TED2021-129652B-C21, funded by MICIU/AEI/10.13039/501100011033 and by "European Union NextGenerationEU/PRTR". The authors would like to thank the following mechanical engineering students for their help with the experimental work: E. Díez and A. Lizán; also to E. Sánchez for his excellent work as a laboratory technician and especially to N & N for their collaboration inside and outside the laboratory.

References

[1] IEA, The Future of Cooling: Opportunities for Energy-Efficient Air Conditioning, International Energy Agency, Paris, 2018, http://dx.doi.org/10.1787/9789264301993-en.
[2] A. Chel, G. Kaushik, Renewable energy technologies for sustainable development of energy efficient building, Alex. Eng. J. 57 (2) (2018) 655–669, http://dx.doi.org/10.1016/j.aej.2017.02.027.
[3] EU, World Leader in Renewables, Energy Efficiency First, EU Commission, 2017, URL: https://energy.ec.europa.eu/system/files/2017-01/energy_union_package_factsheet_iv_v2_0.pdf.
[4] D. Mugnier, R. Fedrizzi, R. Thygesen, T. Selke, New generation solar cooling and heating systems with IEA SHC Task 53: Overview and first results, Energy Procedia 70 (2015) 470–473, http://dx.doi.org/10.1016/j.egypro.2015.02.149, International Conference on Solar Heating and Cooling for Buildings and Industry, SHC 2014.
[5] F. Aguilar, S. Aledo, P. Quiles, Experimental analysis of an air conditioner powered by photovoltaic energy and supported by the grid, Appl. Therm. Eng. 123 (2017) 486–497, http://dx.doi.org/10.1016/j.applthermaleng.2017.05.123.
[6] R. Opoku, K. Mensah-Darkwa, A. Samed Muntaka, Techno-economic analysis of a hybrid solar PV-grid powered air-conditioner for daytime office use in hot humid climates – A case study in Kumasi city, Ghana, Sol. Energy 165 (2018) 65–74, http://dx.doi.org/10.1016/j.solener.2018.03.013.
[7] C. Lorenzo, L. Narvarte, R. Almeida, A. Cristóbal, Technical evaluation of a stand-alone photovoltaic heat pump system without batteries for cooling applications, Sol. Energy 206 (2020) 92–105, http://dx.doi.org/10.1016/j.solener.2020.05.097.
[8] Y. Chen, Y. Liu, J. Liu, X. Luo, D. Wang, Y. Wang, J. Liu, Design and adaptability of photovoltaic air conditioning system based on office buildings, Sol. Energy 202 (2020) 17–24, http://dx.doi.org/10.1016/j.solener.2020.03.055.
[9] I. Saâd, S. Maalej, M.C. Zaghdoudi, Performance of a hybrid solar PV-grid-powered domestic air conditioner, in: 20th International Multi-Conference on Systems, Signals and Devices, SSD, 2023, http://dx.doi.org/10.1109/SSD58187.2023.10411318.
[10] O. Ayadi, B. Rinchi, F. Alsaleem, Experimental evaluation of a solar-powered air conditioner, Sol. Energy 272 (2024) http://dx.doi.org/10.1016/j.solener.2024.112466.
[11] H. Li, H. Zhang, B. Zou, J. Peng, A generalized study of photovoltaic driven air conditioning potential in cooling season in Mainland China, Renew. Energy 223 (2024) 120048, http://dx.doi.org/10.1016/j.renene.2024.120048.
[12] S. He, H. Gurgenci, Z. Guan, X. Huang, M. Lucas, A review of wetted media with potential application in the pre-cooling of natural draft dry cooling towers, Renew. Sustain. Energy Rev. 44 (2015) 407–422, http://dx.doi.org/10.1016/j.rser.2014.12.037.
[13] N.I. Ibrahim, A.A. Al-Farayedhi, P. Gandhidasan, Experimental investigation of a vapor compression system with condenser air pre-cooling by condensate, Appl. Therm. Eng. 110 (2017) 1255–1263, http://dx.doi.org/10.1016/j.applthermaleng.2016.09.042.
[14] F.W. Yu, W.T. Ho, K.T. Chan, R.K.Y. Sit, Theoretical and experimental analyses of mist precooling for an air-cooled chiller, Appl. Therm. Eng. 130 (2018) 112–119, http://dx.doi.org/10.1016/j.applthermaleng.2017.11.046.
[15] H. Yang, L. Rong, X. Liu, L. Liu, M. Fan, N. Pei, Experimental research on spray evaporative cooling system applied to air-cooled chiller condenser, Energy Rep. 6 (2020) 906–913, http://dx.doi.org/10.1016/j.egyr.2020.04.001.
[16] T.A. Jacob, N. Shah, W.Y. Park, Evaluation of hybrid evaporative-vapor compression air conditioners for different global climates, Energy Convers. Manage. 249 (2021) http://dx.doi.org/10.1016/j.enconman.2021.114841.
[17] S.K. Gupta, B. Arora, A. Arora, Thermodynamic performance assessment of air conditioner combining evaporative and passive cooling, J. Therm. Sci. Eng. Appl. 16 (5) (2024) http://dx.doi.org/10.1115/1.4064743.
[18] I. Atmaca, A. Senol, A. Çaglar, Performance testing and optimization of a split-type air conditioner with evaporatively-cooled condenser, Eng. Sci. Technol. Int. J. 32 (2022) http://dx.doi.org/10.1016/j.jestch.2021.09.010.
[19] S.K. Gupta, B. Arora, A. Arora, Thermo-economic assessment of air conditioner utilizing direct evaporative cooling: A comprehensive analysis, Int. J. Refrig. 158 (2024) 68–88, http://dx.doi.org/10.1016/j.ijrefrig.2023.11.021.
[20] P. Martínez, J. Ruiz, C.G. Cutillas, P.J. Martínez, A.S. Kaiser, M. Lucas, Experimental study on energy performance of a split air-conditioner by using variable thickness evaporative cooling pads coupled to the condenser, Appl. Therm. Eng. 105 (2016) 1041–1050, http://dx.doi.org/10.1016/j.applthermaleng.2016.01.067.
[21] K. Harby, F. Al-Amri, An investigation on energy savings of a split air-conditioning using different commercial cooling pad thicknesses and climatic conditions, Energy 182 (2019) 321–336, http://dx.doi.org/10.1016/j.energy.2019.06.031.
[22] Z. Yang, Y. Zhang, H. Xiao, R. Zhuang, X. Liang, M. Cui, X. Li, J. Zhao, Q. Yuan, R. Yang, B. Wang, W. Shi, Comprehensive test of ultra-efficient air conditioner with smart evaporative cooling ventilation and photovoltaic, Energy Convers. Manag. 254 (2022) 115267, http://dx.doi.org/10.1016/j.enconman.2022.115267.
[23] F. Aguilar, D. Neyer, P. Quiles, Monitoring Procedure for Field Test & Demo Systems with Compression Heat Pumps Driven by Photovoltaic Solar Energy, International Energy Agency. Task 53. New Generation Solar Cooling & Heating Systems (PV or solar thermally driven systems), 2019, http://dx.doi.org/10.18777/ieashc-task53-2019-0008, URL: https://api.semanticscholar.org/CorpusID:199091600, Report C1-1.
[24] K. Klein, EES-Engineering Equation Solver, Version 10.836 ND, F-Chart Software, Middleton, 2020.
[25] T. Kuehn, J.L. Threlkeld, J.W. Ramsey, Thermal Environmental Engineering, Prentice Hall, New Jersey, 1998.
[26] JCGM/WG1, Evaluation of Measurement Data – Guide to the Expression of Uncertainty in Measurement. JCGM 100:2008 (GUM 1995 with Minor Corrections), Joint Committee for Guides in Metrology, Paris, 2008, URL: https://www.bipm.org/documents/20126/2071204/JCGM_100_2008_E.pdf.
[27] C. Tran, P. Rivière, D. Marchio, C. Arzano-Daurelle, Refrigerant-based measurement method of heat pump seasonal performances performances, Int. J. Refrig. 35 (6) (2012) 1583–1594, http://dx.doi.org/10.1016/j.ijrefrig.2012.03.010.
[28] R.W. Koca, W.C. Hughes, L.L. Christianson, Evaporative cooling pads: Test procedure and evaluation, Appl. Eng. Agric. 7 (4) (1991) 485–490.
[29] S. He, Z. Guan, H. Gurgenci, K. Hooman, Y. Lu, A.M. Alkhedhair, Experimental study of the application of two trickle media for inlet air pre-cooling of natural draft dry cooling towers, Energy Convers. Manage. 89 (2015) 644–654, http://dx.doi.org/10.1016/j.enconman.2014.10.031.
[30] A. Tejero-González, A. Franco-Salas, Direct evaporative cooling from wetted surfaces: Challenges for a clean air conditioning solution, Wiley Interdiscip. Rev.: Energy Environ. 11 (3) (2022) http://dx.doi.org/10.1002/wene.423.
[31] IDAE, Factores De Emisión De CO_2 Y Coeficientes De Paso a Energía Primaria De Diferentes Fuentes De Energía Final Consumidas En El Sector De Edificios En España, Instituto para la Diversificación y Ahorro de la Energía. Ministerio de Industria Energía y Turismo, 2016.